J. Space Weather Space Clim., 7, A10 (2017)
DOI: 10.1051/swsc/2017007

SWSC

TOPICAL REVIEW OPEN ACCESS

Where does Earth's atmosphere get its energy?

Andrew C. Kren[1,*], Peter Pilewskie[2,3], and Odele Coddington[3]

[1] Colorado State University, Cooperative Institute for Research in the Atmosphere at the NOAA Earth System Research Laboratory/Global Systems Division, 325 Broadway, Boulder, CO 80305, USA
[*]Corresponding author: andrew.kren@noaa.gov
[2] Department of Atmospheric and Oceanic Sciences, University of Colorado Boulder, 4001 Discovery Drive, Boulder, CO 80303, USA
[3] University of Colorado, Laboratory for Atmospheric and Space Physics, 3665 Discovery Drive, Boulder, CO 80303, USA

Received 15 February 2016 / Accepted 15 February 2017

ABSTRACT

The Sun is Earth's primary source of energy. In this paper, we compare the magnitude of the Sun to all other external (to the atmosphere) energy sources. These external sources were previously identified in Sellers (1965); here, we quantify and update them. These external sources provide a total energy to the Earth that is more than 3700 times smaller than that provided by the Sun, a vast majority of which is provided by heat from the Earth's interior. After accounting for the fact that 71% of incident solar radiation is deposited into the earth system, the Sun provides a total energy to Earth that is still more than 2600 times larger than the sum of all other external sources.

Key words. Atmosphere – Ocean – Sun – Energy deposition – Energy distribution

1. Introduction

William D. Sellers book *Physical Climatology*, published in 1965, included a table on large-scale energy sources "that act continuously or quasicontinuously in the atmosphere and at its boundaries" (Table 2 in Sellers 1965). In a number of talks presented by the authors of this paper over the past decade, Sellers' (1965) Table 2 (Table 1 in this paper) has been reproduced to emphasize the overwhelming dominance that solar radiation contributes to Earth's energy budget. On the basis of viewer responses to those presentations, an update to Sellers' table is presented herein (see Table 2) to bring several of the table entries up to date.

There are some noteworthy comments regarding the table. The caption to the table and its discussion in the text imply that the table is not intended to be considered complete. Some of the in situ energy sources in the original table, for example lightning discharges and fossil fuel combustion, appear to be arbitrary, accounting for a small number of important sources that could have been included. For example, convective and latent heat transfer and infrared emission were not in Sellers' list. A footnote to the table suggests that it was intended for comparative purposes: "most of the data in this table and in Table 3 have been obtained from an unpublished series of notes by H.H. Lettau (Department of Meteorology, University of Wisconsin)".[1]

In this paper, we attempted to maintain fidelity to the original intent of the table, giving primary attention to the same sources in Sellers (1965). The origins of most of the sources are external to the atmosphere and therefore, provide the intended context to the question, *where does the atmosphere get its energy?* That the list of internal sources is incomplete is of minor consequence. After all, in equilibrium these must balance the input from the Sun and other external sources since they are redistributions of those sources. A more complete accounting of internal sources can be found in other, widely referenced studies by Wild et al. (2013), Stephens et al. (2012), and Trenberth et al. (2009). Finally, it was not our intention to provide a complete literature review of the various sources of energy. The range of physical processes underlying the generation and dissipation of these energy sources requires an endeavor far beyond the scope of this paper.

The following Section 2 provides the background for the revisions to each of the terms in the original table. In Section 3, we provide a few external sources of energy that were not included in the original Sellers table.

2. Updates to Sellers' large-scale energy sources

Here we provide the basis for updates to the entries in Sellers' (1965) Table 2 (and shown in Table 2 in this paper). Each source is discussed in a subsection with the exception of lunar reflection and emission, which are combined in a single section. Note that the energy from these sources is deposited at depths varying from near the top-of-the-atmosphere (if there is such a thing) to the Earth's surface, necessitating a common reference depth to compare flux densities from different sources. Unless otherwise noted, flux densities are derived for a reference sphere of radius equal to Earth's mean radius; that is, the reference depth is at the surface. When measurement or model uncertainties were found in the published literature they were included in our updated values. In other cases, ranges of estimates are listed to provide either minimum to maximum power inputs for a given source or estimates from multiple references. In most (but not all) instances we resist explaining differences between our updated values and Sellers' original estimates because there

[1] In contrast to the focus here on large-scale (global) energy sources, Table 3 in Sellers (1965) lists the energy associated with localized processes in the atmosphere.

Table 1. Energy sources from Sellers (1965) and relative to that of the Sun (final column). Relative input calculated with respect to the flux density values (middle column). Values are global averages.

Energy source	Flux density [W m^{-2}]	Relative to total solar irradiance
Solar irradiance	**348.93**[1]	**1.000**
Earth's interior heat flux	0.0612	1.8×10^{-4}
Infrared radiation from the full Moon	0.0102	2.9×10^{-5}
Reflected radiation from the full Moon	0.0034	9.7×10^{-6}
Solar atmospheric tides	0.0034	9.7×10^{-6}
Combustion of coal, oil, and gas in the United States	0.0024	6.9×10^{-6}
Lightning discharge energy	2.0×10^{-4}	5.7×10^{-7}
Magnetic storm dissipation	6.8×10^{-5}	1.9×10^{-7}
Auroral emission	4.8×10^{-5}	1.4×10^{-7}
Cosmic radiation	3.1×10^{-5}	8.9×10^{-8}
Dissipation of energy from micrometeorites	2.0×10^{-5}	5.7×10^{-8}
Total radiation from stars	1.4×10^{-5}	4.0×10^{-8}
Lunar tides	1.0×10^{-5}	2.9×10^{-8}
Zodiacal irradiance	3.4×10^{-6}	9.7×10^{-9}

[1] Sellers provided solar irradiance (what he called the *solar constant*) in units of kilo-Langley (kly) per year; 1 kly $year^{-1}$ is 1.3267 W m^{-2}. The value he cited for globally averaged solar irradiance was 263 kly $year^{-1}$.

Table 2. Revised energy sources from current study. Flux density and relative input values are defined the same as in Table 1. Values are global averages, and where applicable, are mean values over the solar cycle. The solar irradiance value is globally averaged at 1 AU. The third column from left is the estimated uncertainty, if known; in some cases, a range is reported from the literature. See text for further discussion. The fifth column lists the section number of each energy source.

Energy source	Flux density [W m^{-2}]	Uncertainty or range [W m^{-2}]	Relative to total solar irradiance	Section number
Solar irradiance	**340.2**	**±0.12**	**1.000**	**2.1**
Earth's interior heat flux	0.09	±0.006	2.6×10^{-4}	2.2
Infrared radiation from the full Moon	0.01	8.7×10^{-3} to 0.0113	2.9×10^{-5}	2.3
Combustion of coal, oil, and gas in the United States	0.0052	–	1.5×10^{-5}	2.4
Magnetic storm dissipation	0.00362	1.0×10^{-5} to 1.0×10^{-3}	1.1×10^{-5}	2.5
Reflected radiation from the full Moon	0.0018	1.57×10^{-3} to 2.03×10^{-3}	5.3×10^{-6}	2.3
Solar atmospheric tides	0.00168	–	4.9×10^{-6}	2.6
Lightning discharge energy	4.95×10^{-4}	9.0×10^{-5} to 9.0×10^{-4}	1.5×10^{-6}	2.7
Auroral emission	3.7×10^{-4}	1.0×10^{-5} to 1.0×10^{-3}	1.1×10^{-6}	2.8
Zodiacal irradiance	5.67×10^{-5}	5.65×10^{-5} to 5.68×10^{-5}	1.7×10^{-7}	2.9
Lunar tides	1.96×10^{-5}	–	5.8×10^{-8}	2.10
Total radiation from stars	6.78×10^{-6}	5.62×10^{-6} to 7.94×10^{-6}	2.0×10^{-8}	2.11
Cosmic microwave background radiation	3.13×10^{-6}	$\pm 2.62 \times 10^{-9}$	9.2×10^{-9}	2.12
Dissipation of energy from micrometeorites	1.1×10^{-6}	1.9×10^{-8} to 2.0×10^{-6}	3.2×10^{-9}	2.13
Additional external sources				
Airglow emission	0.0036	–	1.1×10^{-5}	3
Galactic cosmic rays	8.5×10^{-6}	7.0×10^{-6} to 1.0×10^{-5}	2.5×10^{-8}	3
Earthshine	1.93×10^{-7}	–	5.7×10^{-10}	3

is no way of determining how Sellers derived his values. Sellers and Lettau are deceased.

2.1. Solar irradiance

The Sun impacts the Earth and its atmosphere in a variety of ways and to differing degrees. The Sun's influence extends from the farthest reaches of Earth's magnetic field where charged particles from the Sun interact with Earth's magnetosphere, all the way down to Earth's surface. Here we present the Sun's dominant energy input to the Earth, solar irradiance, or radiant flux density. The most accurate measurement of the spectrally integrated solar irradiance, called Total Solar Irradiance (TSI), provided by Kopp & Lean (2011),

is 1360.8 W m^{-2}. Distributed uniformly over the Earth's surface (globally averaged) this amounts to 340.2 ± 0.12 W m^{-2}. This is the basis of reference for all of the other energy sources discussed in this section. Contrast this with Sellers' (1965) value of 348.9 W m^{-2}, more than a decade before the first measurements of TSI from space.

Solar irradiance varies on timescales from minutes to eons (Willson & Hudson 1988; Hoyt & Schatten 1997; Usoskin et al. 2007; Solanki et al. 2013), due to the turbulent convection-induced dynamical motions and magnetic phenomena within the Sun (Charbonneau 2014) and the rotation of the Sun over a 27-day period (Fröhlich & Lean 2004). The top-of-the-atmosphere solar irradiance, or TSI, varies by approximately 0.1% over the 11-year solar cycle (Willson & Hudson 1991; Lean 1997; Fröhlich 2006; Kopp 2014). This energy is distributed across the entire spectrum from gamma rays (10^{-10} m) to radiowaves (>10^{2} m), although 97% of the total energy occurs between 200 and 2400 nm (Harder et al. 2009). Figure 1 shows the solar spectrum measured by the Spectral Irradiance Monitor (SIM) (Harder et al. 2005) onboard NASA's Solar Radiation and Climate Experiment (SORCE) satellite. Solar Spectral Irradiance (SSI) ranges from roughly 0.5 W m^{-2} nm^{-1} at 310 nm, to a maximum of around 2 W m^{-2} nm^{-1} at around 500 nm. SSI exhibits the greatest *relative* variability over the solar cycle at ultraviolet (UV) wavelengths; for example, the relative variability of irradiance in the extreme UV is over 100 times that of TSI, and there is very little variability in the infrared (Floyd et al. 2003; Ermolli et al. 2013 and references therein).

While TSI constrains the magnitude of solar variability, the Earth's climate response to the solar variability is wavelength dependent. Within Earth's atmosphere and its surface, the incoming solar energy is scattered and absorbed in unique, wavelength-dependent ways. The impact of solar variability on climate is thought to be a combination of several factors, many of which are beyond the scope of this paper. The reader is referred to Ermolli et al. (2013), Solanki et al. (2013), and Gray et al. (2010) for recent reviews of solar influences on climate.

2.2. Earth's interior heat flux

The Earth is constantly emitting thermal energy (heat) from its interior and crust into the atmosphere and global oceans. Current estimates of the total heat flux from Earth's interior are 44.2 ± 1.0 × 10^{12} W (Pollack et al. 1993; Gando et al. 2011) and 46 ± 3 × 10^{12} W (Jaupart et al. 2015) with 32 ± 2 × 10^{12} W lost through the ocean floor and 14 ± 1 × 10^{12} W lost through continental areas (Jaupart et al. 2015). It is estimated that approximately half of this energy comes from radioactive decay of four primary elements: Uranium 238, Uranium 235, Thorium 232, and Potassium 40, and subsequent conduction and convection from the crust, mantle, and core (Fowler 1990; Stacey & Davis 2008); the remaining flux is likely due to *primordial heat* from gravitational energy during the formation of the Earth, which continues to cool since its formation (Fowler 1990; Gando et al. 2011).

There are estimates of the magnitude and spatial distribution (Fig. 2) of global heat loss. These estimates of global heat loss, summarized in Jaupart et al. (2015), span 41–47 × 10^{12} W and are made using data sets of heat flux observations (Fig. 3) and, for the oceans, a combination of measurements with an improved theoretical thermal model

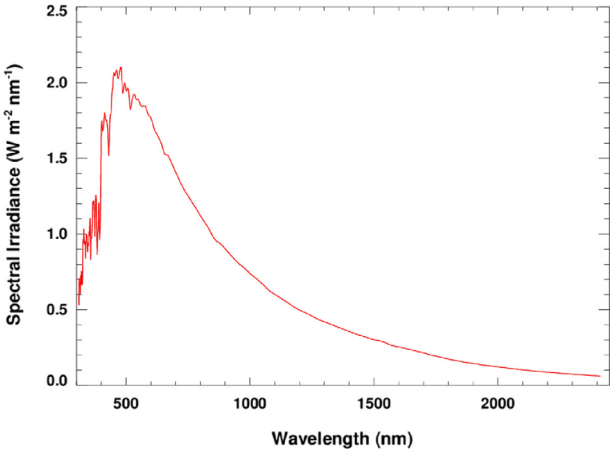

Fig. 1. Solar spectral irradiance (SSI; W m^{-2} nm^{-1}) measured by the SIM instrument (Harder et al. 2005) between 300 and 2400 nm.

validated against local measurements (Williams & Von Herzen 1974; Davies 1980a, 1980b; Sclater et al. 1980; Pollack et al. 1993; Davies & Davies, 2010; Jaupart et al. 2015). The thermal model is used to quantify the additional heat transfer by hydrothermal convective circulation (Stein & Stein, 1992) (i.e., in addition to the conductive ocean heat measured at heat flux observation sites), particularly in regions of young seafloors that are characterized by fractured crust and larger and more variable heat flows. Estimates of the energy released from Earth's interior made from observations alone are smaller, ranging from 29 to 34 × 10^{12} W (Hofmeister & Criss 2005; Hamza et al. 2008).

Using the estimate from Jaupart et al. (2015) of 46 ± 3 × 10^{12} W, we obtain an average surface flux density of 0.09 ± 0.006 W m^{-2}. We note the change from Sellers' (1965) estimate of 0.0612 W m^{-2} is likely attributable to the improvement in the number, location, and quality of measurements, improvements in hydrothermal circulation models, and improved understanding of uncertainties as identified in Jaupart et al. (2015) and references within.

2.3. Infrared and reflected radiation from the full Moon

It was difficult and in most cases, impossible, to determine the sources of differences between our updated estimates and those from Sellers' original table. Lunar emission and scattering of sunlight are two of the entries where we could reproduce exactly what Sellers estimated, making some common assumptions: the Moon emits as a blackbody and it is a perfect diffuser, scattering isotropically. In principle, neither assumption is true but they provide the basis for making a simple estimate.

Using these assumptions and simple energy balance, the emitted irradiance at the Moon's surface, F_E, averaged over the sunlit side of the full Moon is:

$$F_E = \frac{(1 - a_M)S_0}{2}, \quad (1)$$

where a_M is the lunar albedo and S_0 is the normally incident solar irradiance, or TSI. The reflected irradiance at the Moon's surface, F_R, averaged over the sunlit hemisphere is:

$$F_R = \bar{\mu} a_M S_0 \quad (2)$$

where the average cosine of solar zenith angle, $\bar{\mu}$, is 0.5. While the respective irradiances, F_E and F_R, contributing

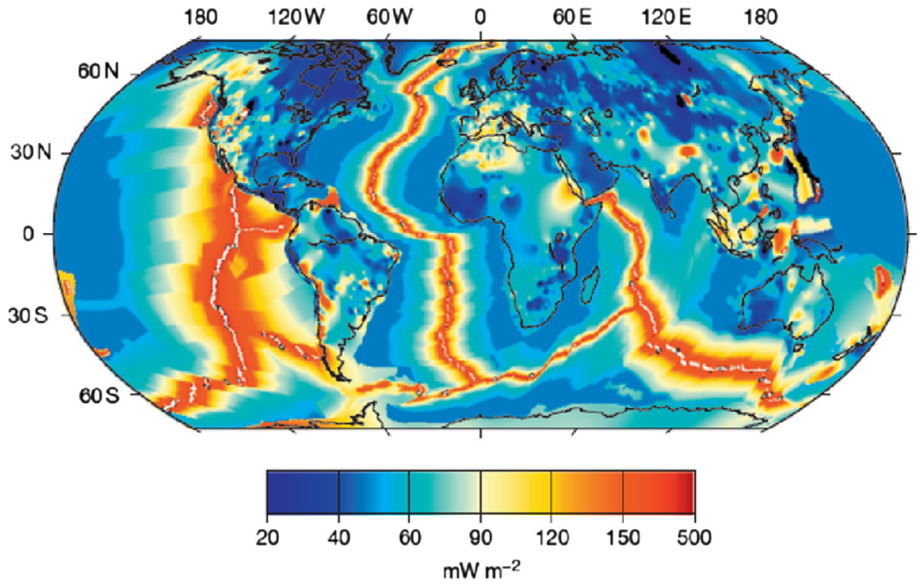

Fig. 2. Contributions of total global heat flux over land and ocean in mW m^{-2} based on observations and a thermal model, which is used to determine the cooling of the oceanic lithosphere. Figure reprinted from Jaupart et al. (2015), with permission from Elsevier, license number 3984240052236.

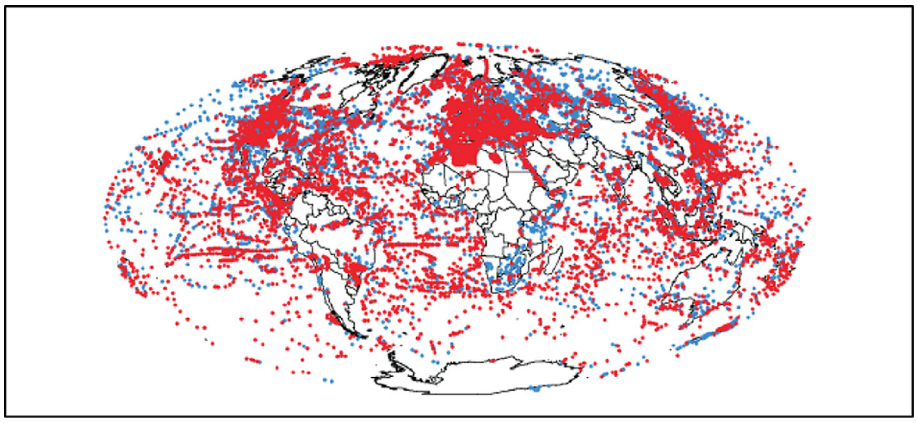

Fig. 3. The global observing network of observing sites for measuring the heat flow from Earth's interior. Red dots denote the Davies & Davies (2010) study with 55% more observing sites than the Pollack et al. (1993) study. From Davies & Davies (2010). Reproduced with permission from J. H. Davies.

to Earth's energy budget would diminish by an amount proportional to the inverse of the square of the distance between Earth and Moon, the ratio of emitted to reflected irradiance is invariant with distance and is simply:

$$\frac{F_E}{F_R} = \frac{1 - a_M}{a_M}. \quad (3)$$

Sellers' estimate of this ratio is exactly 3, indicating that he assumed a lunar albedo of 0.25, considerably higher than modern estimates closer to 0.1. For example, Matthews (2008) published a measured lunar albedo of 0.1362. Using this value, the ratio of emitted to reflected full Moon radiation is more than a factor of 6. To determine the value for both lunar irradiances requires TSI (S_0) at the Moon, assumed to be the same as for Earth, 1360.8 W m^{-2} (Kopp & Lean 2011). Using equations (1) and (2) we estimate a full Moon emitted irradiance of 588 W m^{-2} and reflected solar irradiance of 93 W m^{-2}. These simple estimates can be compared to measurements from the Clouds and the Earth's Radiant Energy System (CERES) Terra and Aqua satellite observations (Matthews 2008), which reported 977 W m^{-2} and 180 W m^{-2} for emitted and reflected irradiance, respectively, at 7° phase angle. To compare with the hemispherical-averaged values from our estimates, both measured irradiances are divided by 2, to arrive at 488.5 W m^{-2} for full Moon emission and 90 W m^{-2} for reflected solar irradiance. The latter is remarkably close to our simple estimate that used the same measured lunar albedo from Matthews (2008). There is a much larger difference, approximately 20%, between our simple estimate and measured lunar emission from CERES. This may be explained by measurements of lunar emissivity that differ significantly from unity over much of the infrared spectrum (Murcray 1965; Murcray et al. 1970).

Because in our simple model we assumed that the Moon scatters solar radiation isotropically and emits as a blackbody and therefore, also emits isotropically, scattered and emitted *radiances* are F_R/π and F_E/π, respectively. Furthermore,

because the solid angle that the Moon subtends at the Earth is much less than unity, we approximate the lunar irradiances incident on the Earth by the product of lunar radiance and the solid angle of the Moon, 6.5×10^{-5} steradians. Using the CERES measurements of irradiances averaged over the full sunlit Moon we arrive at 0.010 W m^{-2} for full Moon emission and 0.0018 W m^{-2} for full Moon solar reflected irradiance incident on the Earth. Note that these values were derived for the mean of the Earth-Moon distance, which varies by approximately 13% over the orbit (Allen 1973), meaning that the full Moon emitted and reflected irradiance incident at Earth will vary by approximately 27%.

2.4. Combustion of coal, oil, and gas in the United States

The Sellers (1965) value of heat flux from combustion of coal, oil, and gas in the United States was 0.0024 W m^{-2} when globally distributed. To update, we used data for the consumption measurements of coal, oil, and gas over the continental United States for the year 2015 archived at the United States Energy Information Administration (EIA) (http://www.eia.gov). Since 1950, consumption of these resources in the U.S. has increased from 31 quadrillion British Thermal Units (BTUs) to approximately 79 quadrillion BTUs, leading to an updated flux density of 0.0052 W m^{-2}. For a global non-renewable energy consumption estimate, including nuclear, we cite Flanner (2009) for the year 2005 to derive a flux density of 0.028 W m^{-2}.

2.5. Magnetic storm dissipation

Geomagnetic storms are caused by high-speed streams of the solar wind that increase the flux of energetic particles entering the magnetosphere, creating an enhanced ring current formed by ions and electrons that circle the Earth (Gonzalez et al. 1994) and causing a change in Earth's magnetic field (Akasofu 1978; Gonzalez et al. 1994; Kamide et al. 1998; Eddy 2009; Lopez et al. 2009). Coronal Mass Ejections (CMEs) and to a lesser extent, coronal holes, are primarily responsible for geomagnetic storms (Gosling et al. 1991; Kamide et al. 1998). CMEs, which are most prevalent during solar maximum (Kamide et al. 1998), are intense bursts of the solar wind that can reach speeds of 2000 km s^{-1} (Gosling & Forsyth 2001) and rise above the solar corona. Coronal holes, more prevalent during solar minimum, are regions of anomalously low density and temperature in the solar corona that emit plasma at speeds of 750–800 km s^{-1} (Zirker 1977; Kamide et al. 1998). Magnetic storms are principal drivers of major disturbances on Earth, such as power system blackouts and phone system outages (Boteler et al. 1998; Pulkkinen 2007). However, we also have magnetic storms to thank for the creation of beautiful aurorae in the night sky.

There are different pathways for the dissipation of energy from geomagnetic storms (Weiss et al. 1992; Slinker et al. 1995; Silbergleit et al. 1997; Lu et al. 1998; Slavin et al. 1998). The partitioning of the magnetic storm dissipation energy can be estimated using multiple techniques including ground and satellite-based observations of energy fluxes, empirical formulas (e.g., Pulkkinen et al. 2002; Li et al. 2012), model simulations (Palmroth et al. 2004; Tanskanen et al. 2005; Ngwira et al. 2013), and assimilation techniques (Lu et al. 1998). In empirical methods, for example, estimates of the solar wind input energy, a function of solar wind speed and solar magnetic field orientation and strength (Silbergleit et al. 1997) is used to determine the energy input into the magnetosphere (Gonzalez et al. 1994; Pulkkinen et al. 2002). In-situ measurements of the precipitation of auroral particles (Pulkkinen et al. 2002) can be used in combination with auroral models to estimate magnetic storm energy. Assimilation techniques such as the Assimilative Mapping of Ionospheric Electrodynamics (AMIE) method can also be used to study magnetic storm energy and dissipation; in one particular case it was shown that 400 GW (1 GW = 1.0×10^9 W) of energy was deposited during a magnetic storm and partitioned such that 190 GW went into Joule heating, 120 GW into ring current injection, and 90 GW into auroral precipitation (Lu et al. 1998).

Numerous studies have estimated the power dissipation in magnetic storms (e.g., Akasofu 1978; Stern 1984; Akasofu & Kamide 1985; Weiss et al. 1992; Lu et al. 1995; Knipp et al. 1998; Lu et al. 1998; Baker et al. 1997; Silbergleit et al. 1997; Baker et al. 2001; Pulkkinen et al. 2002; Tanskanen et al. 2002; Feldstein et al. 2003; Palmroth et al. 2004; Tanskanen et al. 2005; Alex et al. 2006; Guo et al. 2011; Li et al. 2012; Akasofu 2013). There is a wide range in dissipative energies due to the varying strength of the solar wind and geomagnetic indices, storm duration, as well as the technique used to derive the global power. These dissipative energies range from ~10^{10}–10^{11} W for substorm events, which are much weaker both in physical extent and energy than magnetic storms (Echer et al. 2011), 10^{11}–10^{12} W for moderate storm events, to 10^{12}–10^{13} W during intense geomagnetic events (Li et al. 2012).

The average magnetic storm flux density dissipation that spans substorm through intense geomagnetic activity is 0.00399 W m^{-2} when distributed over the Earth's surface. Auroral emission is included in this estimate. Since Sellers (1965) treated auroral emission separately from geomagnetic storm dissipation, we remove the average auroral flux density equal to 3.7×10^{-4} W m^{-2} (see Sect. 2.8 for details) from the average magnetic storm flux density. The resulting global average flux density for magnetic storm dissipation, excluding the auroral component, is 0.00362 W m^{-2} and the range in values spans ~10^{-5} W m^{-2} to ~10^{-3} W m^{-2}. The Sellers (1965) estimate of 6.8×10^{-5} W m^{-2} falls within this range.

2.6. Solar atmospheric tides

The Sun imparts a tidal force on Earth's atmosphere through radiative heating of the atmosphere and surface and latent heat release via global scale convection (Zhang et al. 2010a, 2010b). Additional sources of tidal forcing come from nonlinear interactions between planetary waves (McLandress 2002), interactions between gravity waves and tides (McLandress & Ward 1994), and to a lesser extent, by the gravitational force of the Sun on the Earth (Hagan & Forbes 2002). Each of these components modifies the dynamical motion of the upper atmosphere through temperature and wind perturbations. The solar tides are one of the dominant features present in the mesosphere and lower thermosphere (Chapman & Lindzen 1970; Oberheide et al. 2002).

Radiative and latent heating components due to the Sun produce tidal oscillations and amplitudes that can be found at both diurnal and semi-diurnal timescales, with additional components often ignored due to their smaller contributions (Chapman & Lindzen 1970). This heating, the vast majority of which originates in the troposphere, generates vertically propagating internal gravity waves that arise from density

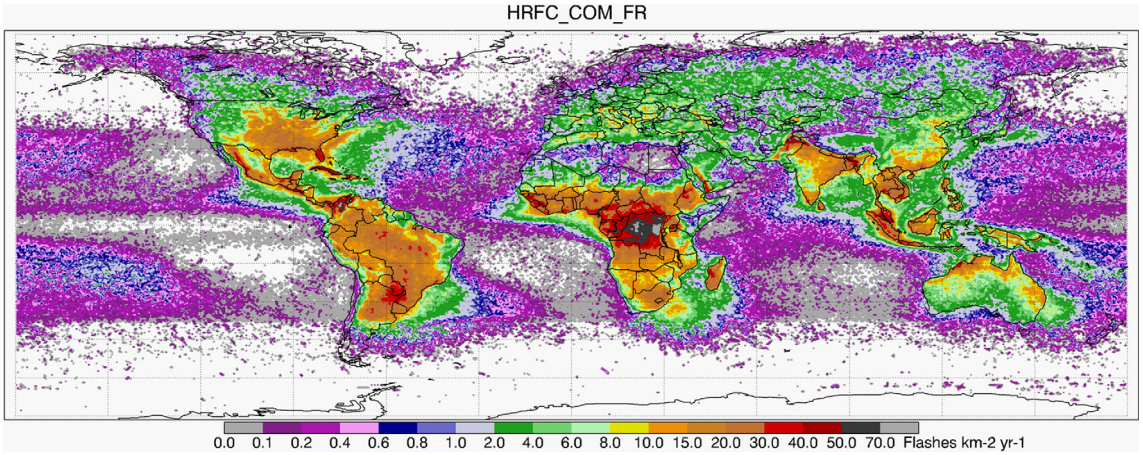

Fig. 4. The annualized distribution of total lightning activity derived from the Optical Transient Detector (OTD) and Lightning Imaging Sensor (LIS) in units of flashes km^{-2} yr^{-1}. Figure updated from Cecil et al. (2014) and provided by Daniel Cecil to include data through 2013.

fluctuations (Holton 2004). These waves propagate vertically into the upper atmosphere, where their growth and amplitudes increase exponentially, influencing the large-scale global circulation patterns through temperature, pressure, and wind modulation (Oberheide et al. 2002; Zhang et al. 2010a). These waves dissipate and reach maximum amplitude in the mesosphere and lower thermosphere at altitudes between 80 and 120 km (Zhang et al. 2010a).

At the surface, heating from sensible and latent heat fluxes over land and ocean can induce pressure amplitudes of approximately 1.3 hPa (Dai & Wang 1999). In the mesosphere and lower thermosphere, satellite observations of radiative flux and temperature, as well as tidal and general circulation models, indicate amplitudes of the solar atmospheric tide on zonal mean temperature and winds ranging from 10 to 40 K and 20 to 60 ms^{-1}, respectively (Forbes 1982b; Angelats & Forbes 2002; Hagan & Forbes 2002; Forbes et al. 2006, 2008; Hagan et al. 2009; Zhang et al. 2010a, 2010b).

Groves & Forbes (1984) estimated the energy dissipated within the atmosphere by the diurnal and semi-diurnal solar tidal forces. First, they calculated the time averaged and subsequent global mean vertical energy flux deposited in the upper atmosphere using a numerical tidal model from the surface to 400 km, which included temperature, pressure, wind, and vertical velocity fields derived by Forbes (1982a). This tidal model incorporated background wind and temperature fields, atmospheric composition, eddy and molecular diffusion, and tidal forcing through realistic water vapor and ozone heating rates in the upper atmosphere (Forbes 1982a). Globally averaged, the solar diurnal and equinox semi-diurnal components of the vertical energy flux are 1.64×10^{-3} W m^{-2} and 0.044×10^{-3} W m^{-2}, together yielding a global average at Earth's surface of 1.68×10^{-3} W m^{-2} (Groves & Forbes 1984), roughly 50% smaller than the estimate from Sellers (1965) of 3.4×10^{-3} W m^{-2}.

2.7. Lightning discharge energy

Global sensible and latent heat fluxes transport heat and moisture vertically into the atmosphere, providing energy to fuel thunderstorms. The majority of lightning is associated with these convective thunderstorms (Uman 1987; MacGorman & Rust 1998; Rakov & Uman 2003). The original source of these energy fluxes is, of course, the Sun.

The first estimate of global lightning frequency was performed by Brooks (1925). This estimate was derived by compiling a climatological survey of thunderstorm frequency over the globe, obtained from meteorological stations and ocean ship logs. Data was primarily available over central Europe and eastern North America. Using a flash rate measured from a single storm in England in June 1908, Brooks (1925) applied his thunderstorm climatology to infer global lightning flash rate as a function of season, latitude, ocean, and land (Orville & Spencer 1979). He obtained an average global frequency of 100 flashes s^{-1}. This value was well accepted until the satellite observations commenced in the 1960s (Orville & Spencer 1979). Estimates of lightning frequency from satellites using photometers, photographs, and lightning detectors (e.g., Sparrow & Ney 1968, 1971; Orville & Spencer 1979; Kotaki & Katoh 1983; Mackerras et al. 1998) showed a wide range in frequency, from 14 to 400 flashes s^{-1} (Orville & Spencer 1979; Mackerras et al. 1998; Schumann & Huntrieser 2007). Most of these estimates were hampered by a limited observational period, taken primarily at night, over selected regions, and exhibited low detection efficiency (Christian et al. 2003). This led to uncertainties in the frequency of lightning over diurnal, seasonal, and annual time periods.

More recent space-borne measurements of lightning frequency establish global lightning flash rates of 44 ± 5 flashes s^{-1} based on a 5-year climatology using day and night intra-cloud and cloud-to-ground flash observations from NASA's Optical Transient Detector (OTD) on board the Microlab-1 satellite (OV-1) (Christian et al. 2003). Cecil et al. (2014) updated the global lightning flash climatology to 46 flashes s^{-1}, varying seasonally from 35 flashes s^{-1} in February, to 60 flashes s^{-1} in August, by merging data from the OTD sensor (1995–2000) with the Lightning Imaging Sensor (LIS) on the Tropical Rainfall Measuring Mission (TRMM) satellite from 1998 to 2010. Figure 4 shows the annually averaged global distribution of total lightning activity (flashes km^{-2} yr^{-1}) from 1995 to 2013 (Cecil et al. 2014, with data updated through 2013). The majority of lightning flashes occur in the tropics and over land, where the storm updrafts are most intense to produce electrification (Zipser 1994). Approximately 1.46 billion flashes occur annually over the Earth (Cecil et al. 2014).

We derived the global power per unit area dissipated by lightning discharges by multiplying the average amount of energy per single lightning flash by the global lightning frequency. Using the Cecil et al. (2014) estimate of 46 flashes s^{-1} and the dissipative range of energy per flash of 10^9–10^{10} J (Price et al. 1997), the total power dissipated globally by lightning per year is 4.6×10^{10} to 4.6×10^{11} W. This corresponds to a global power per unit area between 9×10^{-5} and 9×10^{-4} W m^{-2}, with an average of 4.95×10^{-4} W m^{-2}. Sellers' (1965) estimate of 2.0×10^{-4} W m^{-2} is within this range.

2.8. Auroral emission

The aurora is a luminous emission that takes place in the upper part of the atmosphere (Liu et al. 2008). It is driven by the interaction between Earth's magnetic field and solar energetic particles carried by the solar wind (Vazquez & Vaquero 2010). When the solar energetic particles interact with atomic and molecular nitrogen and oxygen at altitudes between 90 and 150 km, the excited nitrogen and oxygen atoms and molecules emit excess energy and drop into a lower energy state, producing the auroral light (Bone 2007). These energetic particles also produce upper atmospheric warming, ionization, dissociation, and recombination, as well as increased horizontal wind velocity and the generation of vertical winds (Christensen et al. 1997; Hecht et al. 2006; Oyama et al. 2010). These energetic particles therefore play a significant role in the chemistry of the upper stratosphere to the lower mesosphere (Seppälä et al. 2006; Pulkkinen 2007; Jackman et al. 2009). The predominant particles responsible for the auroral precipitation are charged electrons in the 1–30 keV range (Bone 2007), with charged protons contributing ~10–15% of the total (Hardy et al. 1989; Emery et al. 2008). The aurora occurs in both the northern (aurora borealis) and southern (aurora australis) polar regions.

Since the 1970s, measurements of the auroral emission and energy fluxes have been available from global satellite observations (e.g., Hardy et al. 1985; Fuller-Rowell & Evans 1987; Torr et al. 1995; Germany et al. 1997; Frey et al. 2001; Christensen et al. 2003; Emery et al. 2008; Hecht et al. 2008; Liou 2010). The global auroral power can be calculated directly by the in-situ energy flux measurements, indirectly by incorporating the observed emissions into auroral models, or through empirical relationships between the auroral brightness and energy flux (e.g., Newell et al. 2001, 2009; Emery et al. 2008).

We obtain a direct estimate of the auroral emission, over the 275–815 nm spectral range by using observations from the Optical Spectrograph and InfraRed Imager System (OSIRIS) spectrograph on the Odin spacecraft (Gattinger et al. 2009, 2010). OSIRIS measures the limb brightness of the aurora at 1 nm resolution at a tangent altitude of 105 km (Gattinger et al. 2009). We spectrally integrate OSIRIS aurora spectra at a single latitude and longitude from 2003 (Gattinger et al. 2009; Fig. 1) and 2005 (Gattinger et al. 2010; Fig. 1) and obtain 0.044 W m^{-2} and 0.060 W m^{-2}, respectively. To convert these values to a global auroral emission, we make the following assumptions. First, the width of the auroral oval is 6.5° extending from 60.5° to 67° N (Akasofu 1966; Rostoker & Skone 1993); we compute the surface area bounded by these latitude and longitudes at an altitude of 105 km above Earth to be equal to 1.27×10^{13} m^2. Second, the aurora does not vary in time or space so the point values of auroral emission obtained using the Gattinger et al (2009; 2010) data are representative of all latitudes and longitudes within the defined auroral oval. Therefore, the conversion from hemispheric to global auroral power is a factor of 2. Using these assumptions, the global auroral power derived from the OSIRIS point values is 1.12×10^{12} W and 1.52×10^{12} W, respectively. By taking the average of these values and then another average over Earth's surface area, we derive an average global auroral flux density of 2.6×10^{-3} W m^{-2}.

Using the same set of assumptions given above, we use a point value of auroral emission of 0.018 W m^{-2} (Chamberlain 1961; Table 5.5) to compute an average global average auroral flux density of 8.96×10^{-4} W m^{-2}. Similarly, measurements of three intense geomagnetic storms in October and November 2003 were shown to provide an average global auroral power dissipation of 613 GW (Alex et al. 2006); we used this value to derive a global average auroral flux density of 1.2×10^{-3} W m^{-2}.

The range in auroral flux densities varies with the time rate of change of magnetic activity acting on the magnetosphere. The planetary index, K_p, is representative of the time rate of change of magnetic activity where large values of K_p indicate intense magnetic and auroral activity (Dessler & Fejer 1963). Hubert et al. (2002) derived hemispheric auroral power for four magnetic storm events in 2000 and related these to K_p level by matching the observed in-situ energy flux measurements to climatological energy flux maps (based on K_p levels 0–5+; Fuller-Rowell & Evans 1987). The hemispheric power ranges from ~20 GW for K_p of 3 to as high as 115 GW for K_p of 6 (Hubert et al. 2002). Luan et al. (2010) found a similar range in hemispheric auroral power as a function of K_p level from ~5 years of satellite measurements (~30 GW for K_p 3 to ~92 GW for K_p 6). Again, using the same set of assumptions listed above, we converted the Hubert et al. (2002) auroral power values to energy flux densities as a function of K_p index to obtain a range in globally averaged auroral flux densities from 7.8×10^{-5} W m^{-2} for K_p of 3 to 4.5×10^{-4} W m^{-2} for K_p of 6.

Our ranges in auroral flux densities were derived using assumptions that affect the accuracy of our estimations. We assumed the aurora is hemispherically symmetrical, which it is not (Laundal & Østgaard 2009; Luan et al. 2010). We also assumed that the auroral emission at one latitude and longitude is representative of all locations within the auroral oval, but there is spatial and seasonal variability (Miyashita et al. 2005; Coumans et al. 2004; Luan et al 2010). Given these caveats, we provide an estimate of the ranges in globally averaged auroral flux density equal to ~10^{-5} W m^{-2} to 10^{-4} W m^{-2} (for K_p levels of 3 to 6) to ~10^{-3} W m^{-2} (for intense geomagnetic activity). An average, over all geomagnetic activity levels, is 3.7×10^{-4} W m^{-2}. The Sellers (1965) estimate of 4.8×10^{-5} W m^{-2} falls within this range.

2.9. Zodiacal irradiance

The zodiacal irradiance (or light) is sunlight scattered from the zodiacal cloud, which is composed of micron to millimeter sized particles of interplanetary dust distributed between the Sun and the orbit of the asteroid belt and orbiting the Sun in a disk along the ecliptic (Edberg & Levy 1994; Fixsen & Dwek 2002; Ishiguro et al. 2013). It is visible to the naked eye as a bright column of light above the horizon and can be seen in the evening after sunset and in the morning before sunrise (Leinert 1975; Grün & Dikarev 2009).

The greatest density of dust particles is found closest to the Sun; at 2.5 AU the zodiacal light brightness is <3% of that observed at 1 AU (Tsumura et al. 2010): contributions beyond 3.3 AU are negligible (Hanner et al. 1974). The particles are lost by gravitational entrainment by the Sun (the Poynting-Robertson drag effect), collisions with other dust particles, planetary perturbations, and momentum exchange with the solar wind (Fixsen & Dwek 2002; Yang & Ishiguro 2015). These loss mechanisms are compensated by dust produced through impacts or ice sublimation (Yang & Ishiguro 2015).

The emission and scattering of radiation by the zodiacal dust cloud is wavelength dependent. Peak scattering occurs at 0.5 μm (Leinert et al. 1998). At 3.6 μm, the scattering and emission contributions are roughly equal (Krick et al. 2012). Emission dominates in the mid to far infrared reaching peak values between 10 and 12 μm. The spectral distribution of zodiacal light follows closely the solar spectrum in the visible, but is slightly shifted to longer wavelengths (Tsumura et al. 2010). In the infrared, the emission approximates that of a blackbody with a temperature between 280 and 286 K (Kelsall et al. 1998; Wright 1998). A comparison of observations (Reach et al. 2003) to zodiacal light models shows qualitative agreement to within 10%.

Here we calculate the zodiacal radiation by using measurements of the zodiacal radiance in the visible (0.55 μm) and infrared (12 μm) from Grün & Dikarev (2009) at various ecliptic latitudes and longitudes. The solar spectrum from 0.25 μm to 10 μm is used to scale the scattered radiance in the shortwave and a blackbody curve from 0.35 μm to 100 μm with peak emission at 12 μm to scale the emitted radiance. Although the measurements from Grün & Dikarev (2009) were made over one-quarter of the celestial sphere, the zodiacal cloud is approximately symmetric with respect to the ecliptic plane (Leinert et al. 1998). Integrating the normal component of the broadband shortwave and longwave radiances, $L(\theta, \phi)$, over the solid angle of one-quarter of the celestial sphere, and multiplying by a factor of 4 (to account for the full celestial sphere) gives a total irradiance, F:

$$F = 4\int_{\phi=0}^{\pi} \mathrm{d}\phi \int_{\theta=0}^{\frac{\pi}{2}} L\cos(\theta) sin(\theta)\mathrm{d}\theta. \quad (4)$$

We compute a range in the infrared zodiacal radiation bounded by dust temperatures of 280 K and 286 K and report the total irradiance as the sum of scattered and emitted contributions. We find an average total zodiacal irradiance of 5.67×10^{-5} W m^{-2}, ranging from 5.65×10^{-5} W m^{-2} to 5.68×10^{-5} W m^{-2}. This value was obtained from the sum of the total emission component of 4.715×10^{-5} W m^{-2}, which is an average total infrared emission from a zodiacal dust cloud with temperatures spanning 280 to 286 K (4.73×10^{-5} W m^{-2} to 4.7×10^{-5} W m^{-2}, respectively), and a scattered light component of 9.54×10^{-6} W m^{-2}.

Our computed value is an order of magnitude larger than Sellers' (1965) estimate of 3.4×10^{-6} W m^{-2}. It is plausible that the Sellers (1965) estimate did not consider the component of infrared emission from the dust grains due to a lack of emission measurements until the 1970s (Leinert et al. 2002). However, we note that our method of scaling the scattered and emitted components based on measurements at two wavelengths could result in a larger integrated energy value.

2.10. Lunar tides

The Moon produces oscillations in the atmosphere due to the gravitational interaction of the Earth and Moon (Chapman & Lindzen 1970). These atmospheric tides are considerably smaller in amplitude than the dominant, atmospheric thermal tide of the Sun (Chapman & Lindzen 1970; Vial & Forbes 1994; Sandford et al. 2006). The dominant component of the lunar atmospheric tide is the M_2 tide with a period of 12.42 h (Chapman & Lindzen 1970; Sandford et al. 2006; Forbes et al. 2013). According to Chapman & Lindzen (1970), there are as many as 30 components comprising the lunar tide, most of which are much smaller in amplitude and, therefore, are often ignored due to the limited ability of measurements to detect their small signal (Sandford et al. 2006).

Platzman (1991) performed an energy balance study of the lunar atmospheric tide by incorporating the three factors of the ocean, body, and load tides, characterized by barometric pressure data from Haurwitz & Cowley (1969) and satellite altimeter data of sea-tide dissipation and sea-tide elevation from NASA's Geodetic Satellite (Geosat) (Cartwright & Ray, 1990). The energy dissipated in the atmosphere due to the lunar atmospheric tide was determined as the sum of excitation energy from the Moon's gravitational effect on the body and load tides and by the vertical flux of tidal energy the atmosphere receives from the ocean (Platzman 1991). Annually averaged results showed that the lunar atmospheric tidal dissipation was on the order of 10 GW and maintained almost entirely by the ocean tide (Platzman 1991). This value corresponds to 1.96×10^{-5} W m^{-2} when averaged at Earth's surface. This value is roughly 50% larger than that of Sellers (1965).

2.11. Total radiation from stars

Radiation from stars originates from beyond the heliosphere within the Milky Way galaxy. It is estimated that the Milky Way galaxy contains about 10^{11} stars, with a total mass of 2×10^{41} kg (Gonzalo 2008). Measuring the radiation from stars is difficult due to foreground sources from airglow and zodiacal light (e.g., Brandt & Draine 2012; Arai et al. 2015).

The energy density of starlight spans the ultraviolet through the infrared. Models of stellar emission between 0.09 and 0.245 μm use a power-law approximation and between 0.245 and 8 μm, a sum of three dilute blackbodies with dilution factor "W", and temperature "T" (Mathis et al. 1983; Draine 2011; Brandt & Draine 2012). The dilution factor is the ratio of energy density "u", to the energy density of the undiluted blackbody radiation temperature. The different blackbody temperatures reflect the emission from stars at different stages in their life cycle and the dilution factor, typically $\ll 1$, reflects the dilution of the radiation over great distances (Mathis et al. 1983; Draine 2011). The relationship between stellar radiation energy density and temperature for a dilute blackbody is:

$$u = WaT^4 \quad (5)$$

where the astrophysical radiation constant, a, is equal to $4\sigma/c$ (7.565767×10^{-16} J m^{-3} K^{-4}), σ is the Stefan-Boltzmann constant (5.67×10^{-8} W m^{-2} K^{-4}), and c is the speed of light.

Various studies have reported values for the stellar radiation density. In Table 3, we summarize the radiation energy density values for a selection of these studies (see references listed in table) and convert them to a flux density.

Table 3. Stellar radiation energy densities derived from four different literature sources derived using equation (5) using the published blackbody temperatures and dilution factors (listed in the table) and converted to flux density using the Stefan-Boltzmann law. Note that various studies adopt different numbering for the blackbody temperatures; here, we adopt a numbering scheme that increases with increasing stellar temperature. For a 5th literature source, we derived the stellar flux density from a reported value of stellar mean radiation intensity (see table comments).

Blackbody temperatures (K)	Dilution factors	Radiation energy density (J m^{-3})	Flux density (W m^{-2})	Reference	Comments
$T_1 = 3000$ $T_2 = 4000$ $T_3 = 7500$	$W_1 = 4 \times 10^{-13}$ $W_2 = 1 \times 10^{-13}$ $W_3 = 1 \times 10^{-14}$	$u_1 = 2.45 \times 10^{-14}$ $u_2 = 1.94 \times 10^{-14}$ $u_3 = 2.39 \times 10^{-14}$ (*)For $0.09 < \lambda < .245$ μm $= 7.11 \times 10^{-15}$	$F_1 = 1.83 \times 10^{-6}$ $F_2 = 1.45 \times 10^{-6}$ $F_3 = 1.80 \times 10^{-6}$ $F_{UV} = 5.33 \times 10^{-7}$ $F_{total} = 5.62 \times 10^{-6}$	Mathis et al. (1983)	(*) We modeled the UV radiation as a blackbody.
$T_1 = 3000$ $T_2 = 4000$ $T_3 = 7500$	(Y)$W_1 = 7 \times 10^{-13}$ $W_2 = 1.65 \times 10^{-13}$ $W_3 = 1 \times 10^{-14}$	$u_1 = 4.29 \times 10^{-14}$ $u_2 = 3.20 \times 10^{-14}$ (β)$u_3 = 2.39 \times 10^{-14}$ (*)For $0.09 < \lambda < .245$ μm $= 7.11 \times 10^{-15}$	$F_1 = 3.22 \times 10^{-6}$ $F_2 = 2.40 \times 10^{-6}$ $F_3 = 1.80 \times 10^{-6}$ $F_{UV} = 5.33 \times 10^{-7}$ $F_{total} = 7.94 \times 10^{-6}$	Draine (2011)	(*) We modeled the UV radiation as a blackbody. (Y) Draine (2011) increased this dilution factor relative to Mathis et al. (1983) to better agree with Cosmic Background Explorer (COBE) Diffuse Infrared Background Experiment (DIRBE) photometry. (β) Our derived value differs from Draine (2011) (Table 12.1).
		Mean radiation intensity (for $0.09 < \lambda < 8$ μm) = 1.69×10^{-2} erg s^{-1} cm^{-2} (α)$u = 5.63 \times 10^{-14}$	$F_{total} = 5.87 \times 10^{-6}$	Mezger (1990)	(α) We converted to J m^{-2} s^{-1} and divided by the speed of light to convert to a radiation energy density. We treated the radiation as blackbody.
$T_1 = 4000$ $T_2 = 7500$ $T_3 = 14{,}500$	$W_1 = 1.5 \times 10^{-13}$ $W_2 = 1.5 \times 10^{-14}$ $W_3 = 4.0 \times 10^{-16}$	$u_1 = 2.91 \times 10^{-14}$ $u_2 = 3.60 \times 10^{-14}$ $u_3 = 1.34 \times 10^{-14}$	$F_1 = 2.18 \times 10^{-6}$ $F_2 = 2.7 \times 10^{-6}$ $F_3 = 1.0 \times 10^{-6}$ $F_{total} = 5.87 \times 10^{-6}$	Werner & Salpeter (1969)	
$T_1 = 10{,}000$	$W_1 = 1.0 \times 10^{-14}$	$u_1 = 7.57 \times 10^{-14}$	$F_{total} = 5.67 \times 10^{-6}$	Eddington (1926) (as reported in Mezger 1990)	

Relevant comments necessary to interpret our derivations are noted in the rightmost column.

We report an average flux density of Milky Way starlight of 6.78×10^{-6} W m^{-2} derived from an average of stellar flux densities computed using the blackbody temperatures and dilution factors reported in Draine (2011) and Mathis et al. (1983) (see first and second rows of Table 3). This estimate corresponds to an effective blackbody temperature for the Milky Way starlight of 3.31 K. The range of stellar flux densities in Table 3 spans 5.62×10^{-6} W m^{-2} to 7.94×10^{-6} W m^{-2}. Our average stellar flux density estimate is approximately 50% smaller than the Sellers (1965) estimate of 1.4×10^{-5} W m^{-2}, which would correspond to an effective blackbody temperature of 3.96 K.

2.12. Cosmic microwave background radiation

The spectral distribution of energy within the Milky Way galaxy and beyond (*extragalactic*) covers gamma rays through radio waves (e.g., Draine 2011; Cooray 2016). However, theoretical calculations (discussed below) provide evidence that the Cosmic Microwave Background (CMB) was the sole contributor to cosmic radiation considered by Sellers (1965).

The CMB is of extragalactic origin (Cooray 2016). Recent precision measurements (de Bernardis 2015 and references therein) support the theory that the CMB is the remnant of the big bang (Noterdaeme et al. 2011), "of a time when the universe was very hot, which has now cooled down by its expansion" (Stanev 2004). It is universal and radiates almost entirely isotropically (Draine 2011; Bucher 2015), with peak energy in the microwave region (500 μm–5 cm; Fixsen et al. 1996).

Radiation in equilibrium with its surroundings, *blackbody* radiation, is described by the Planck distribution, the spectral integral of which is the Stefan-Boltzmann law, relating temperature "T", to the radiative energy density "u":

$$u = aT^4, \tag{6}$$

or equivalently, temperature to irradiance, F:

$$F = \sigma T^4 \tag{7}$$

σ is the Stefan-Boltzmann constant (5.67×10^{-8} W m^{-2} K^{-4}), and the astrophysical radiation constant

"a" is equal to $4\sigma/c$ (7.565767×10^{-16} J m^{-3} K^{-4}), c is the speed of light.

Measurements from space (Fixsen et al. 1996; Fixsen 2009) yield a CMB temperature of 2.72548 ± 0.00057 K (Fixsen 2009). From equations (6) and (7), the total energy density of CMB radiation is 4.17×10^{-14} J m^{-3} and the flux density at the top-of-the-atmosphere is 3.13×10^{-6} W m^{-2}, with an uncertainty of $\pm 2.62 \times 10^{-9}$ W m^{-2}.

This is an order of magnitude smaller than the Sellers (1965) estimate of 3.1×10^{-5} W m^{-2}, which would arise from a CMB temperature of 4.8 K, in close agreement with the theoretical estimate of the CMB temperature of 5 K by Alpher & Herman (1948). The first measurement of the CMB temperature, 3.5 ± 1.0 K, by Penzias & Wilson (1965) likely came too late to be included in Sellers' table.

2.13. Dissipation of energy from micrometeorites

Micrometeorites are micron to millimeter (~20 μm–2 mm) sized particles (Love & Brownlee 1993; Duprat et al. 2007). They are descendants of meteoroids, objects that are considered to be parent bodies of asteroids and comets (Norton & Chitwood 2008; Plane 2012). The majority of micrometeoroids (~50–90%) either burn up through vaporization or melt upon entering Earth's atmosphere (Ceplecha et al. 1998; Taylor et al. 1998; Maurette 2006; Bardeen et al. 2008), exceeding temperatures of 1900 K (Love & Brownlee 1991). However, if they are sufficiently small, less than 100 μm in diameter (Taylor et al. 1998; Love & Brownlee 1991), and traveling less than ~20 km s^{-1} (Love & Brownlee 1991), they avoid vaporization on entry and make their way to Earth's surface (Fraundorf 1980; Edberg & Levy 1994).

The review by Plane (2012) and references therein of estimates of the global mass influx of Interplanetary Dust Particles (IDP) into Earth's atmosphere show variations in the measurements by more than a factor of 50, ranging from 5×10^3 kg day^{-1} to 2.7×10^5 kg day^{-1}. These come from a variety of measurements, ranging from space-borne dust detectors, radar and lidar, aircraft, satellites, as well as accumulation of meteoric dust on deep sea sediments and ice cores (Grün et al. 1983; Brownlee 1985; Wasson & Kyte 1987; Love & Brownlee 1993; Ceplecha et al. 1998; Mathews et al. 2001; Brown et al. 2002; Janches et al. 2006; Maurette 2006; Plane 2012). In addition to the broad range of global mass influx, the entry velocity of IDPs is found to exhibit a bimodal nature, ranging between a slow (~15 km s^{-1}) and fast (~55 km s^{-1}) component (Janches et al. 2006 and references within).

Plane (2012) suggests three ranges in the mass influx and entry velocity of IDP based on various measurements and modeling. First, a low range of meteoroid mass influx between 5×10^3 kg day^{-1} and 1×10^4 kg day^{-1} with an entry velocity less than 15 km s^{-1}. Second, a medium range in mass influx between $\sim 2 \times 10^4$ kg day^{-1} and 5×10^4 kg day^{-1} with an average micrometeorite entry velocity of greater than 20 km s^{-1}. Third, an upper range in mass influx between 1×10^5 kg day^{-1} and 3×10^5 kg day^{-1}.

To compute the mechanical energy dissipated by the passage of micrometeorites through Earth's atmosphere, we assume the kinetic energy of their passage is equivalent to their mechanical energy. We use representative mass influx values, m, for low, medium, and high influx conditions as defined by the average of the respective mass influx ranges defined in Plane (2012). We use typical entry velocities, v, of 15 km s^{-1}, 55 km s^{-1}, and ~30 km s^{-1} representative of the low, medium, and high categories from Janches et al. (2006). Our calculations, presented as daily average power estimates, give values of 9.8×10^6 W, 6.1×10^8 W, and 1.0×10^9 W for the low, medium, and high categories, respectively. When the power is globally averaged at Earth's surface, the flux of dissipated mechanical energy is 1.9×10^{-8} W m^{-2}, 1.2×10^{-6} W m^{-2}, and 2.0×10^{-6} W m^{-2} for low, medium, and high categories, respectively. The average of these flux values is 1.1×10^{-6} W m^{-2}, an order of magnitude smaller than the Sellers (1965) estimate. The wide range in daily global mass influx (10^3–10^5 kg day^{-1}) and entry velocities (15–55 km s^{-1}) of these micrometeoroids is one possible reason for the discrepancies in these two values. Also, earlier estimates for the influx rates of meteoroid material were larger (~10^6 kg day^{-1}; Hawkins 1956; Hawkins & Upton 1958). These earlier estimates were deduced from radio echo and photographic observations, producing an energy dissipation in line with the Sellers (1965) value.

3. Some other external sources

There are a few omissions in Sellers' original table that warrant discussion: airglow, galactic cosmic rays, and Earthshine.

Airglow is emission from Earth's upper atmosphere between altitudes of 80 and 300 km induced by absorption of solar radiation by various atmospheric constituents (Chamberlain 1961; Leinert et al. 1998; Khomich et al. 2008). The subsequent excitation, dissociation, recombination, and ionization of these species produce emissions of light known as airglow (Meinel 1951; Meier 1991; Khomich et al. 2008). Airglow emission over the 0.1–0.9 μm range was estimated using spectra of the dayglow (Broadfoot et al. 1997) and nightglow from the Arizona Airglow Experiment (GLO) flown on the space shuttles STS-53 (December 1992) and STS-74 (November 1995; Broadfoot & Bellaire 1999). We determined the airglow emission by spectrally integrating the dayglow (0.1–0.9 μm) and nightglow (0.24–0.9 μm) brightness curves that were provided by Lyle Broadfoot (personal communication). We assumed that the airglow does not vary spatially (not always true; see Gao et al., 2016) and emission is isotropic. We calculate for the dayglow and nightglow values of 4.82×10^{-3} W m^{-2} and 2.37×10^{-3} W m^{-2}, respectively; an average of these values, 3.6×10^{-3} W m^{-2}, is similar in magnitude to that reported by Khomich et al. (2008).

Pertsev & Perminov (2008) using ground-based observation data at Moscow, Russia from 2000 to 2006, report solar cycle variations of 30–40% in hydroxyl (OH) and molecular oxygen; seasonal variations were also found. Gao et al. (2016) analyzed 13 years (2002–2015) of globally averaged nightglow emissions at selected wavelength bands in the infrared from nitrogen oxide (NO) at 5.3 μm, OH at 1.6 and 2.0 μm, and oxygen (O_2) at 1.27 μm using data from the Sounding of the Atmosphere using Broadband Emission Radiometry (SABER) and Solar Extreme Ultraviolet Experiments (SEE) on the Thermosphere-Ionosphere-Mesosphere Energetics and Dynamics (TIMED) satellite (Mlynczak 1997); these measurements show variability over the 11-year solar cycle of ~12% in OH, ~22% in O_2, and ~176% in NO.

Galactic Cosmic Rays (GCRs) are charged particles, predominantly protons, that originate outside the solar system,

most likely from supernova explosions (Blasi 2013). They continually bombard the Earth's atmosphere with energies sufficiently high (approximately 10^7 eV to 10^{21} eV) to influence various altitude-dependent atmospheric phenomena based on the magnitude of the GCR energies (Mironova et al. 2015). These influences can be primary or secondary in nature. A primary effect is when ionization energy is released when a GCR particle is absorbed within the atmosphere. Secondary effects occur when collisions between GCR particles and atmospheric gases produce elementary charged particles, such as electrons, gamma-rays, and mesons that cascade down to lower altitudes (Bazilevskaya 2000). The influx of GCRs into the solar system and Earth's atmosphere is affected predominantly by the Sun's magnetic cycle; the GCR flux is out of phase with this magnetic cycle (Mironova et al. 2015). Shorter term, episodic, modulation in GCRs can also occur from releases of energy from the Sun's photosphere (i.e. solar flares) or from the Sun's corona (i.e. coronal mass ejections) that cause disturbances that "sweep away" the GCRs (Bazilevskaya 2000). Earth's magnetic field may also act as a shield, deflecting cosmic rays toward the poles along field lines due to their partially charged nature (NRC 1994; Bazilevskaya et al. 2008).

Globally averaged GCR flux densities into the Earth's atmosphere are on the order of 7.0×10^{-6} to 1.0×10^{-5} W m^{-2} (NRC 1994; Bazilevskaya 2000; Bazilevskaya et al. 2000) with an average of 8.5×10^{-6} W m^{-2}; ground observations place solar cycle variability of GCRs at 4–15% whereas upper-atmosphere balloon observations record solar cycle variability of 45% or greater (NRC 1994; Mironova et al. 2015).

Earthshine, also known as ashen light, is "the glow of the 'dark' part of the lunar disk that is visible to a nighttime observer" (Goode et al. 2001). It is the amount of sunlight that is reflected by the Earth onto the Moon and then reflected from the Moon back onto the Earth. It is of interest here not because it is a significant energy source but because it can be used to estimate Earth's albedo (Goode et al. 2001). Bohren & Clothiaux (2006) give the ratio of full Moon to new Moon to be 9300. From this, and assuming that the ratio of full and new Moon spectral reflectance scale the same as it does in the visible, we estimate the magnitude of Earthshine to be full Moon reflected irradiance 0.0018 W m^{-2} (from Sect. 2.3) divided by 9300, or 1.93×10^{-7} W m^{-2}.

4. Summary

We provide updates to Sellers' (1965) Table 1 of large-scale energy sources that act continuously or quasicontinuously in the atmosphere and at its boundaries. The original intent of our referencing this table was to compare the sum of all external (to the atmosphere) energy sources to the Sun. If we exclude lightning discharges and fossil fuel combustion, we see that the rate of energy provided by the Sun is over 3000 times greater than all other sources. Going one step further, eliminating all sources that represent transformations of solar energy (lunar emission and reflection, magnetic storms, airglow, solar tides, and zodiacal light), the ratio of solar to non-solar sources is almost 3800. Even after recognizing that only a fraction, 0.71 (e.g. Wild et al. 2013), of solar energy is deposited into (absorbed by) the Earth system, that amount still exceeds the energy from all other external sources by a factor of approximately 2700. In the absence of the Sun, the radiative equilibrium temperature of the Earth (assumed to be a blackbody) would be approximately 36 K.

Acknowledgements. This work was supported under NOAA Award NA09NES4400016 and NASA Award NNX15AK59G. We would like to thank in particular Richard Blakeslee, Geoff Crowley, Gang Lu, Mike Hauser, Richard Arendt, Lyle Broadfoot, Bob Meier, Bruce Draine, Jeff Forbes, Harmut Spetzler, Jonathan Fentzke, Eberhard Gruen, Rebecca Bernstein, Dirk Lummerzheim, E. J. (Ted) Llewellyn, Dan Baker, Sebastian Schmidt, J. Huw Davies, Galina Bazilevskaya, Thomas Kelsall, J. Scott Evans, Christoph Leinert, and Dale Fixsen, who have provided insight, guidance, and suggestions on the many energy sources described in this paper. We would also like to thank the editors and the two anonymous reviewers, whose comments and suggestions helped to greatly improve the manuscript. The editor thanks two anonymous referees for their assistance in evaluating this paper.

References

Akasofu, S.-I. The auroral oval, the auroral substorm, and their relations with the internal structure of the magnetosphere. *Planet. Space Sci.*, **14**, 587–595, 1966.

Akasofu, S.-I. Magnetospheric substorms. *Eos Trans. AGU*, **59**, 68–73, 1978.

Akasofu, S.-I. The relationship between the magnetosphere and magnetospheric/auroral substorms. *Ann. Geophys.*, **31**, 387–394, 2013, DOI: 10.5194/angeo-31-387-2013.

Akasofu, S.-I., and Y. Kamide. Meridian chains of magnetometers as a powerful "remote sensing" tool in determining electromagnetic quantities in the ionosphere on a global scale. *Eos Trans. AGU*, **66 (22)**, 465–466, 1985, DOI: 10.1029/EO066i022p00465.

Alex, S., S. Mukherjee, and G.S. Lakhina. Geomagnetic signatures during the intense geomagnetic storms of 29 October and 20 November 2003. *J. Atmos. Solar Terr. Phys.*, **68**, 769–780, 2006, DOI: 10.1016/j.jastp.2006.01.003.

Allen, C.W. Astrophysical quantities, 3rd edn., Athlone Press, London, 310, 1973.

Alpher, R.A., and R. Herman. Evolution of the Universe. *Nature*, **162**, 774–775, 1948, DOI: 10.1038/162774b0.

Angelats, M., and J.M. Forbes. Nonlinear interactions in the upper atmosphere: the s = 1 and s = 3 nonmigrating semidiurnal tides. *J. Geophys. Res.*, **107 (A8)**, 1157, 2002, DOI: 10.1029/2001JA900179.

Arai, T., S. Matsuura, J. Bock, A. Cooray, M.G. Kim, et al. Measurements of the mean diffuse galactic light spectrum in the 0.95–1.65 μm band from CIBER. *Astrophys. J*, **806 (69)**, 1–14, 2015, DOI: 10.1088/0004-637X/806/1/69.

Baker, D.N., N.E. Turner, and T.I. Pulkkinen. Energy transport and dissipation in the magnetosphere during geomagnetic storms. *J. Atmos. Solar Terr. Phys.*, **63**, 421–429, 2001.

Baker, D.N., T.I. Pulkkinen, M. Hesse, and R.L. McPherron. A quantitative assessment of energy storage and release in the Earth's magnetotail. *J. Geophys. Res.*, **102 (A4)**, 7159–7168, 1997, DOI: 10.1029/96JA03961.

Bardeen, C.G., O.B. Toon, E.J. Jensen, D.R. Marsh, and V.L. Harvey. Numerical simulations of the three-dimensional distribution of meteoric dust in the mesosphere and upper stratosphere. *J. Geophys. Res.*, **113**, D17202, 2008, DOI: 10.1029/2007JD009515.

Bazilevskaya, G.A. Observations of variability in cosmic rays. *Space Sci. Rev.*, **94**, 25–38, 2000.

Bazilevskaya, G.A., M.B. Krainev, and V.S. Makhmutov. Effects of cosmic rays on the Earth's environment. *J. Atmos. Sol. Terr. Phys.*, **62**, 1577–1586, 2000.

Bazilevskaya, G.A., I.G. Usoskin, E.O. Fluckiger, R.G. Harrison, L. Desorgher, et al. Cosmic ray induced ion production in the atmosphere. *Space Sci. Rev.*, **137**, 149–173, 2008.

Blasi, P. The origin of galactic cosmic rays. *Astron. Astrophys. Rev.*, **21**, 1–87, 2013, DOI: 10.1007/s00159-013-0070-7.

Bohren, C.F., and E.E. Clothiaux. *Fundamentals of atmospheric radiation*, John Wiley & Sons, Inc., Germany, ISBN-10: 3527405039/ISBN-13: 978-3527405039, 2006.

Bone, N. *Aurora: observing and recording nature's spectacular light show*, Springer, New York, NY, USA, ISBN: 978-0-387-68469-7, 2007.

Boteler, D.H., R.J. Pirjola, and H. Nevanlinna. The effects of geomagnetic disturbances on electrical systems at the Earth's surface. *Adv. Space Res.*, **22 (1)**, 17–27, 1998.

Brandt, T.D., and B.T. Draine. The spectrum of the diffuse galactic light: the milky way in scattered light. *Astrophys. J.*, **744 (129)**, 1–13, 2012, DOI: 10.1088/0004-637X/744/2/129.

Broadfoot, A.L., D.B. Hatfield, E.R. Anderson, T.C. Stone, B.R. Sandel, J.A. Gardner, E. Murad, D.J. Knecht, C.P. Pike, and R.A. Viereck. N_2 triplet band systems and atomic oxygen in the dayglow. *J. Geophys. Res.*, **102 (A6)**, 11567–11584, 1997, DOI: 10.1029/97JA00771.

Broadfoot, A.L., and P.J. Bellaire Jr. Bridging the gap between ground-based and space-based observations of the night airglow. *J. Geophys. Res.*, **104 (A8)**, 17127–17138, 1999, DOI: 10.1029/1999JA900135.

Brooks, C.E.P. The distribution of thunderstorms over the globe. *Geophys. Mem. London*, **24**, 147–164, 1925.

Brown, P., R.E. Spalding, D.O. ReVelle, E. Tagliaferri, and S.P. Worden. The flux of small near-Earth objects colliding with the Earth. *Nature*, **420**, 294–296, 2002.

Brownlee, D.E. Cosmic dust: collection and research. *Ann. Rev. Earth Plan. Sci.*, **13**, 147–173, 1985.

Bucher, M. CMB observations in 2015: A status report. *Nucl Part. Phys. Proc.*, **267-269**, 245–253, 2015, DOI: 10.1016/j.nuclphysbps.2015.10.113.

Cartwright, D.E., and R.D. Ray. Oceanic tides from Geosat altimetry. *J. Geophys. Res.*, **95 (C3)**, 3069–3090, 1990, DOI: 10.1029/JC095iC03p03069.

Cecil, D.J., D.E. Beuchler, and R.J. Blakeslee. Gridded lightning climatology from TRMM-LIS and OTD: dataset description. *Atmos. Res.*, **135–136**, 404–414, 2014, DOI: 10.1016/j.atmosres.2012.06.028.

Ceplecha, Z., J. Borovicka, W.G. Elford, D.O. Revelle, R.L. Hawkes, V. Porubcan, and M. Simek. Meteorphenomena and bodies. *Space Sci. Rev.*, **84**, 327–471, 1998.

Chamberlain, J.W. *Physics of the aurora and airglow*, Academic Press, New York, NY, USA, ISBN-10: 1483209105/ISBN-13: 978-1483209104, 1961.

Chapman, S., and R.S. Lindzen. *Atmospheric tides: thermal and gravitational*, Gordon and Breach Science Publishers, New York, NY, USA, ISBN: 978-94-010-3399-2, 1970.

Charbonneau, P. Solar dynamo theory. *Annu. Rev. Astron. Astrophys.*, **52**, 251–290, 2014, DOI: 10.1146/annurev-astro-081913-040012.

Christensen, A.B., J.H. Hecht, R.L. Walterscheid, M.F. Larsen, and W.E. Sharp. Depletion of oxygen in aurora: evidence for a local mechanism. *J. Geophys. Res.*, **102 (A10)**, 22273–22277, 1997, DOI: 10.1029/97JA01800.

Christensen, A.B., L.J. Paxton, S. Avery, J. Craven, G. Crowley, et al. Initial observations with the Global Ultraviolet Imager (GUVI) in the NASA TIMED satellite mission. *J. Geophys. Res.*, **108 (A12)**, 1451, 2003, DOI: 10.1029/2003JA009918.

Christian, H.J., R.J. Blakeslee, D.J. Boccippio, W.L. Boeck, D.E. Buechler, et al. Global frequency and distribution of lightning as observed from space by the Optical Transient Detector. *J. Geophys. Res. Atmos.*, **108**, 4005, 2003, DOI: 10.1029/2002JD002347.

Cooray, A. Extragalactic background light measurements and applications. *R. Soc. Open. Sci.*, **3**, 1–24, 2016.

Coumans, V., J.-C. Gérard, B. Hubert, S.B. Mende, and S.W.H. Cowley. Morphology and seasonal variations of global auroral proton precipitation observed by IMAGE-FUV. *J. Geophys. Res.*, **109**, A12205, 2004, DOI: 10.1029/2003JA010348.

Dai, A., and J. Wang. Diurnal and semidiurnal tides in global surface pressure fields. *J. Atmos. Sci.*, **56**, 3874–3891, 1999, DOI: 10.1175/1520-0469(1999)056<3874:DASTIG>2.0.CO;2.

Davies, G.F. Thermal histories of convective Earth models and constraints on radiogenic heat production in the Earth. *J. Geophys. Res.*, **85**, 2517–2530, 1980a, DOI: 10.1029/JB085iB05p02517.

Davies, G.F. Review of oceanic and global heat flow estimates. *Rev. Geophys.*, **18**, 718–722, 1980b, DOI: 10.1029/RG018i003p00718.

Davies, J.H., and D.R. Davies. Earth's surface heat flux. *Solid Earth*, **1**, 5–24, 2010, DOI: 10.5194/se-1-5-2010.

de Bernardis, P. Precision measurements of the cosmic microwave background. *Nucl. Part. Phys. Proc.*, **265–266**, 48–51, 2015, DOI: 10.1016/j.nuclphysbps.2015.06.013.

Dessler, A.J., and J.A. Fejer. Interpretation of K_p index and M-region geomagnetic storms. *Plan. Space Sci.*, **11**, 505–511, 1963, DOI: 10.1016/0032-0633(63)90074-6.

Draine, B.T. *Physics of the Interstellar and Intergalactic Medium*, Princeton University Press, Princeton, New Jersey, USA, ISBN-10: 0691122148/ISBN-13: 978-0691122144, 2011.

Duprat, J., C. Engrand, M. Maurette, G. Kurat, M. Gounelle, and C. Hammer. Micrometeorites from Central Antarctic snow: the CONCORDIA collection. *Adv. Space Res.*, **39**, 605–611, 2007, DOI: 10.1016/j.asr.2006.05.029.

Echer, E., B.T. Tsurutani, F.L. Guarnieri, and J.U. Kozyra. Interplanetary fast forward shocks and their geomagnetic effects: CAWSES events. *J. Atmos. Sol. Terr. Phys.*, **73**, 1330–1338, 2011, DOI: 10.1016/j.jastp.2010.09.020.

Edberg, S.J., and D.H. Levy. *Observing comets, asteroids, meteors, and the zodiacal light*, Cambridge University Press, New York, NY, USA, ISBN-10: 0521066271/ISBN-13: 978-0521066273, 1994.

Eddington, A.S. *The internal constitution of the stars*, Cambridge University Press, Cambridge, ISBN: 9780521337083, 1926.

Eddy, J.A. *The Sun, the Earth, and near-Earth space*, U.S. Government Printing Office, Washington, DC, 2009.

Emery, B.A., V. Coumans, D.S. Evans, G.A. Germany, M.S. Greer, E. Holeman, K.K. Cade, F.J. Rich, and W. Xu. Seasonal, Kp, solar wind, and solar flux variations in long-term single-pass satellite estimates of electron and ion auroral hemispheric power. *J. Geophys. Res.*, **113**, A0631, 2008, DOI: 10.1029/2007JA012866.

Ermolli, I., K. Matthes, T. Dudok de Wit, N.A. Krivova, K. Tourpali, et al. Recent variability of the solar spectral irradiance and its impact on climate modelling. *Atmos. Chem. Phys.*, **13**, 3945–3977, 2013, DOI: 10.5194/acp-13-3945-2013.

Feldstein, Y.I., L.A. Dremukhina, A.E. Levitin, U. Mall, I.I. Alexeev, and V.V. Kalegaev. Energetics of the magnetosphere during the magnetic storm. *J. Atmos. Solar Terr. Phys.*, **65**, 429–446, 2003, DOI: 10.1016/S1364-6826(02)00339-5.

Fixsen, D.J. The temperature of the cosmic microwave background. *Astrophys. J.*, **707**, 916–920, 2009, DOI: 10.1088/0004-637X/707/2/916.

Fixsen, D.J., E.S. Cheng, J.M. Gales, J.C. Mather, R.A. Shafer, and E.L. Wright. The cosmic microwave background spectrum from the full COBE/FIRAS data set. *Astrophys. J.*, **473**, 576–587, 1996, DOI: 10.1086/178173.

Fixsen, D.J., and E. Dwek. The zodiacal emission spectrum as determined by COBE and its implications. *Astrophys. J.*, **578**, 1009–1014, 2002, DOI: 10.1086/342658.

Floyd, L., G. Rottman, M. DeLand, and J. Pap. 11 years of solar UV irradiance measurements from UARS. In: Wilson, A., Editor. *Solar variability as an input to the Earth's environment. International Solar Cycle Studies (ISCS) Symposium, 23-28 June 2003, Tatranska Lomnica, Slovak Republic*, ESA Publications Division: ESA SP-535, Noordwijk, ISBN: 92-9092-845-X, 2003.

Flanner, M.G. Integrating anthropogenic heat flux with global climate models. *Geophys. Res. Lett.*, **36**, L02801, 2009, DOI: 10.1029/2008GL036465.

Forbes, J.M. Atmospheric tide: 1. Model description and results for the solar diurnal component. *J. Geophys. Res.*, **87 (A7)**, 5222–5240, 1982a, DOI: 10.1029/JA087iA07p05222.

Forbes, J.M. Atmospheric tide: 2. The solar and lunar semidiurnal components. *J. Geophys. Res.*, **87 (A7)**, 5241–5252, 1982b, DOI: 10.1029/JA087iA07p05241.

Forbes, J.M., J. Russell, S. Miyahara, X. Zhang, S. Palo, M. Mlynczak, C.J. Mertens, and M.E. Hagan. Troposphere-thermosphere tidal coupling as measured by the SABER instrument on TIMED during July–September 2002. *J. Geophys. Res.*, **111**, A10S06, 2006, DOI: 10.1029/2005JA011492.

Forbes, J.M., X. Zhang, S. Palo, J. Russell, C.J. Mertens, and M. Mlynczak. Tidal variability in the ionospheric dynamo region. *J. Geophys. Res.*, **113**, A02310, 2008, DOI: 10.1029/2007JA012737.

Forbes, J.M., X. Zhang, S. Bruinsma, and J. Oberheide. Lunar semidiurnal tide in the thermosphere under solar minimum conditions. *J. Geophys. Res.*,**118**, 1788–1801, 2013, DOI: 10.1029/2012JA017962.

Fowler, C.M.R. *The solid Earth: an introduction to global geophysics*, Cambridge University Press, New York, NY, USA, ISBN: 9780521893077, 1990.

Fraundorf, P. The distribution of temperature maxima for micrometeorites decelerated in the Earth's atmosphere without melting. *Geophys. Res. Lett.*, **7 (10)**, 765–768, 1980, DOI: 10.1029/GL007i010p00765.

Frey, H.U., S.B. Mende, C.W. Carlson, J.-C. Gérard, B. Hubert, J. Spann, R. Gladstone, and T.J. Immel. The electron and proton aurora as seen by IMAGE-FUV and FAST. *Geophys. Res. Lett.*, **28 (6)**, 1135–1138, 2001.

Fröhlich, C. Solar irradiance variability since 1978. *Space Sci. Rev.*, **125**, 1–13, 2006, DOI: 10.1007/s11214-006-9046-5.

Fröhlich, C., and J. Lean. Solar radiative output and its variability: evidence and mechanisms. *Astron. Astrophys. Rev.*, **12**, 273–320, 2004, DOI: 10.1007/s00159-004-0024-1.

Fuller-Rowell, T.J., and D.S. Evans. Height-integrated pedersen and hall conductivity patterns inferred from the TIROS-NOAA satellite data. *J. Geophys. Res.*, **92 (A7)**, 7606–7618, 1987, DOI: 10.1029/JA092iA07p07606.

Gando, A., Y. Gando, K. Ichimura, H. Ikeda, K. Inoue, et al. Partial radiogenic heat model for Earth revealed by geoneutrino measurements. *Nature Geosci.*, **4**, 647–651, 2011, DOI: 10.1038/ngeo1205.

Gao, H., J. Xu, and G.-M. Chen. The responses of the nightglow emissions observed by the TIMED/SABER satellite to solar radiation. *J. Geophys. Res.*, **121**,1627–1642, 2016, DOI: 10.1002/2015JA021624.

Gattinger, R.L., A. Vallance Jones, D.A. Degenstein, and E.J. Llewellyn. Quantitative spectroscopy of the aurora. VI. The auroral spectrum from 275 to 815 nm observed by the OSIRIS spectrograph on board the Odin spacecraft. *Can. J. Phys.*, **88**, 559–567, 2010, DOI: 10.1139/P10-037.

Gattinger, R.L., N.D. Lloyd, A.E. Bourassa, D.A. Degenstein, I.C. McDade, and E.J. Llewellyn. Observation of the 557.7 nm to 297.2 nm brightness ratio in the auroral spectrum with OSIRIS on Odin. *Can. J. Phys.*, **87**, 1133–1137, 2009, DOI: 10.1139/P09-102.

Germany, G.A., G.K. Parks, M. Brittnacher, J. Cumnock, D. Lummerzheim, J.F. Spann, L. Chen, P.G. Richards, and F.J. Rich. Remote determination of auroral energy characteristics during substorm activity. *Geophys. Res. Lett.*, **24 (8)**, 995–998, 1997, DOI: 10.1029/97GL00864.

Gonzalez, W.D., J.A. Joselyn, Y. Kamide, H.W. Kroehl, G. Rostoker, B.T. Tsurutani, and V.M. Vasyliunas. What is a geomagnetic storm? *J. Geophys. Res.*, **99 (A4)**, 5771–5792, 1994, DOI: 10.1029/93JA02867.

Gonzalo, J.A. *The intelligible universe: an overview of the last thirteen billion years*, World Scientific Publishing, 2nd edn., Hackensack, NJ, USA, ISBN-13: 978-9812794116, 2008.

Goode, P.R., J. Qiu, V. Yurchyshyn, J. Hickey, M. Chu, E. Kolbe, C.T. Brown, and S.E. Koonin. Earthshine observations of the Earth's reflectance. *Geophys. Res. Lett.*, **28 (9)**, 1671–1674, 2001, DOI: 10.1029/2000GL012580.

Gosling, J.T., D.J. McComas, J.L. Phillips, and S.J. Bame. Geomagnetic activity associated with earth passage of interplanetary shock disturbances and coronal mass ejections. *J. Geophys. Res.*, **96 (A5)**, 7831–7839, 1991, DOI: 10.1029/91JA00316.

Gosling, J.T., and R.J. Forsyth. CME-driven solar wind disturbances at high heliographic latitudes. *Space Sci. Rev.*, **97**, 87–98, 2001, DOI: 10.1023/A:1011874027259

Gray, L.J., J. Beer, M. Geller, J.D. Haigh, M. Lockwood, et al. Solar influences on climate. *Rev. Geophys.*, **48**, RG4001, 2010, DOI: 10.1029/2009RG000282.

Groves, G.V., and J.M. Forbes. Equinox tidal heating of the upper atmosphere. *Planet. Space Sci.*, **32**, 447–456, 1984, DOI: 10.1016/0032-0633(84)90124-7.

Grün, E., H.A. Zook, H. Fechtig, and R.H. Giese. Collisional balance of the meteoric complex. *Icarus*, **62**, 244–272, 1983, DOI: 10.1016/0019-1035(85)90121-6.

Grün, E., and V. Dikarev. Interplanetary dust, Springer, Berlin, Heidelberg, Germany, 501–536, 2009, DOI: 10.1007/978-3-540-88055-4_32.

Guo, J., X. Feng, B.A. Emery, J. Zhang, C. Xiang, F. Shen, and W. Song. Energy transfer during intense geomagnetic storms driven by interplanetary coronal mass ejections and their sheath regions. *J. Geophys. Res.*, **116**, A05106, 2011, DOI: 10.1029/2011JA016490.

Hagan, M.E., A. Maute, and R.G. Roble. Tropospheric tidal effects on the middle and upper atmosphere. *J. Geophys. Res.*, **114**, A01302, 2009, DOI: 10.1029/2008JA013637.

Hagan, M.E., and J.M. Forbes. Migrating and nonmigrating diurnal tides in the middle and upper atmosphere excited by tropospheric latent heat release. *J. Geophys. Res.*, **107**, 4754, 2002, DOI: 10.1029/2001JD001236.

Hamza, V.M., R.R. Cardoso, and C.F. Ponte Neto. Spherical harmonic analysis of Earth's conductive heat flow. *Int. J. Earth Sci.*, **92 (2)**, 205–226, 2008, DOI: 10.1007/s00531-007-0254-3.

Hanner, M.S., J.L. Weinberg, L.M. DeShields II, B.A. Green, and G.N. Toller. Zodiacal light and the asteroid belt: view from Pioneer-10. *J. Geophys. Res.*, **79 (25)**, 3671–3675, 1974.

Harder, J., G. Lawrence, J. Fontenla, G. Rottman, and T. Woods. The spectral irradiance monitor: scientific requirements, instrument design, and operation modes. *Sol. Phys.*, **230**, 141–167, 2005, DOI: 10.1007/0-387-37625-9_9.

Harder, J.W., J.M. Fontenla, P. Pilewskie, E.C. Richard, and T.N. Woods. Trends in solar spectral irradiance variability in the visible and infrared. *Geophys. Res. Lett.*, **36**, L07801, 2009, DOI: 10.1029/2008GL036797.

Hardy, D.A., M.S. Gussenhoven, and D. Brautigam. A statistical model of auroral ion precipitation. *J. Geophys. Res.*, **94 (A1)**, 370–392, 1989, DOI: 10.1029/JA094iA01p00370.

Hardy, D.A., M.S. Gussenhoven, and E. Holeman. A statistical model of auroral electron precipitation. *J. Geophys. Res.*, **90 (A5)**, 4229–4248, 1985, DOI: 10.1029/JA090iA05p04229.

Haurwitz, B., and D. Cowley. The lunar barometric tide, its global distribution and annual variation. *Pure Appl. Geophys.*, **77**, 122–150, 1969, DOI: 10.1007/BF00876008.

Hawkins, G.S. Variation in the occurrence rate of meteors. *Astronom. J.*, **61**, 386–391, 1956, DOI: 10.1086/107367.

Hawkins, G.S., and E.K.L. Upton. The influx rate of meteors in the Earth's atmosphere. *Astrophys. J.*, **128**, 727–735, 1958, DOI: 10.1086/146585.

Hecht, J.H., D.J. Strickland, and M.G. Conde. The application of ground-based optical techniques for inferring electron energy deposition and composition change during auroral precipitation events. *J. Atmos. Solar Terr. Phys.*, **68**, 1502–1519, 2006.

Hecht, J.H., T. Mulligan, D.J. Strickland, A.J. Kocenash, Y. Murayama, et al. Satellite and ground-based observations of auroral energy deposition and the effects on thermospheric

composition during large geomagnetic storms: 1. Great geomagnetic storm of 20 November 2003. *J. Geophys. Res.*, **113**, A01310, 2008, DOI: 10.1029/2007JA012365.

Hofmeister, A.M., and R.E. Criss. Earth's heat flux revised and linked to chemistry. *Tectonophysics*, **395**, 159–177, 2005, DOI: 10.1016/j.tecto.2004.09.006.

Holton, J.R. *An introduction to dynamic meteorology*, Elsevier Academic Press, 2nd edn., San Diego, CA, USA, ISBN-10: 012384660/ISBN-13: 860-1407127349, 2004.

Hoyt, D.V., and K.H. Schatten. *The role of the sun in climate change*, Oxford University Press, New York, NY, USA, ISBN: 0-19-509413-1/ISBN: 0-19-509414-X, 1997.

Hubert, B., J.-C. Gérard, D.S. Evans, M. Meurant, S.B. Mende, H.U. Frey, and T.J. Immel. Total electron and proton energy input during auroral substorms: remote sensing with IMAGE-FUV. *J. Geophys. Res.*, **107 (A8)**, 1183, 2002, DOI: 10.1029/2001JA009229.

Ishiguro, M., H. Yang, F. Usui, J. Pyo, M. Ueno, T. Ootsubo, S.M. Kwon, and T. Mukai. High-resolution imaging of the gegenschein and the geometric albedo of interplanetary dust. *Astrophys. J.*, **767 (1)**, 1–34, 2013, DOI: 10.1088/0004-637x/767/1/75.

Jackman, C.H., D.R. Marsh, F.M. Vitt, R.R. Garcia, C.E. Randall, E.L. Fleming, and S.M. Frith. Long-term middle atmospheric influence on very large solar proton events. *J. Geophys. Res.*, **114**, D11304, 2009, DOI: 10.1029/2008JD011415.

Janches, D., C.J. Heinselman, J.L. Chau, A. Chandran, and R. Woodman. Modeling the global micrometeor input function in the upper atmosphere observed by high power and large aperture radars. *J. Geophys. Res.*, **111**, A07317, 2006, DOI: 10.1029/2006JA011628.

Jaupart, C., S. Labrosse,F.Lucazeau, and J.-C. Mareschal. Temperatures, heat, and energy in the mantle of the earth. Gerald Schubert, Editor-in-cheif. *Treatise on geophysics*, 2nd edn., **vol 7**, Elsevier, Oxford, 223–270, 2015.

Kamide, Y., W. Baumjohann, I.A. Daglis, W.D. Gonzalez, M. Grande, et al. Current understanding of magnetic storms: storm-substorm relationships. *J. Geophys. Res.*, **103 (A8)**, 17705–17728, 1998, DOI: 10.1029/98JA01426.

Kelsall, T., J.L. Weiland, B.A. Franz, W.T. Reach, R.G. Arendt, et al. The COBE diffuse infrared background experiment search for the cosmic infrared background: II. Model of the interplanetary dust cloud. *Astrophys. J.*, **508**, 44–73, 1998, DOI: 10.1086/306380.

Khomich, V.Y., A.I. Semenov, and N.N. Shefov. *Airglow as an indicator of upper atmospheric structure and dynamics*, Springer, Berlin, Heidelberg, Germany, ISBN: 978-3-540-75833-4, 2008.

Knipp, D.J., B.A. Emery, M. Engebretson, X. Li, A.H. McAllister, et al. An overview of the early November 1993 geomagnetic storm. *J. Geophys. Res.*, **103 (A11)**, 26197–26220, 1998, DOI: 10.1029/98JA00762.

Kopp, G. An assessment of the solar irradiance record for climate studies. *J. Space Weather Space Clim.*, **4**, A14, 2014, DOI: 10.1051/swsc2014012.

Kopp, G., and J.L. Lean. A new, lower value of irradiance: evidence and climate significance. *Geophys. Res. Lett.*, **38**, L01706, 2011, DOI: 10.1029/2010GL045777.

Kotaki, M., and C. Katoh. The global distribution of thunderstorm activity observed by the Ionospheric Sounding Satellite (ISS-b). *J. Atmos. Terr. Phys.*, **45**, 843–847, 1983.

Krick, J.E., W.J. Glaccum, S.J. Carey, P.J. Lowrance, J.A. Surace, J.G. Ingalls, J.L. Hora, and W.T. Reach. A Spitzer/IRAC measure of the zodiacal light. *Astrophys. J.*, **754**, 1–5, 2012, DOI: 10.1088/0004-637X/754/1/53.

Laundal, K.M., and N. Østgaard. Asymmetric auroral intensities in the Earth's Northern and Southern hemispheres. *Nature*, **460**, 491–493, 2009, DOI: 10.1038/nature08154.

Lean, J. The Sun's variable radiation and its relevance for Earth. *Annu. Rev. Astron. Astrophys.*, **35**, 33–67, 1997, DOI: 10.1146/annurev.astro.35.1.33.

Leinert, C. Zodiacal light – a measure of the interplanetary environment. *Space Sci. Rev.*, **18**, 281–339, 1975, DOI: 10.1007/BF00212910.

Leinert, C., P. Abraham, J. Acosta-Pulido, D. Lemke, and R. Siebenmorgen. Mid-infrared spectrum of the zodiacal light observed with ISOPHOT. *A&A*, **393**, 1073–1079, 2002, DOI: 10.1051/0004-6361:20021029.

Leinert, C., S. Bowyer, L.K. Haikala, M.S. Hanner, M.G. Hauser, et al. The 1997 reference of diffuse night sky brightness. *Astron. Astrophys. Supp.*, **127**, 1–99, 1998, DOI: 10.1051/aas:1998105.

Li, H., C. Wang, W.Y. Xu, and J.R. Kan. Characteristics of magnetospheric energetics during geomagnetic storms. *J. Geophys. Res.*, **117**, A04225, 2012, DOI: 10.1029/2012JA017584.

Liou, K. Polar Ultraviolet Imager observation of auroral breakup. *J. Geophys. Res.*, **115**, A12219, 2010, DOI: 10.1029/2010JA015578.

Liu, X.-C., G.-X. Chen, W.-Y. Xu, A.-M. Du, Y.-Y. Wu, B. Chen, Y. Wang, and X.-D. Zhao. Relationships of the auroral precipitating particle power with AE and Dst indices. *Chinese J. Geophys.*, **51**, 686–693, 2008, DOI: 10.1002/cjg2.1260.

Lopez, R.E., J.G. Lyon, E. Mitchell, R. Bruntz, V.G. Merkin, S. Brogl, F. Toffoletto, and M. Wiltberger. Why doesn't the ring current injection rate saturate? *J. Geophys. Res.*, **114**, A02204, 2009, DOI: 10.1029/2008JA013141.

Love, S.G., and D.E. Brownlee. Heating and thermal transformation of micrometeoroids entering the Earth's atmosphere. *Icarus*, **89**, 26–43, 1991, DOI: 10.1016/0019-1035(91)90085-8.

Love, S.G., and D.E. Brownlee. A direct measurement of the terrestrial mass accretion rate of cosmic dust. *Science*, **262**, 550–553, 1993, DOI: 10.1126/science.262.5133.550.

Lu, G., A.D. Richmond, B.A. Emery, and R.G. Roble. Magnetosphere-ionosphere-thermosphere coupling: effect of neutral winds on energy transfer and field-aligned current. *J. Geophys. Res.*, **100 (A10)**, 19643–19659, 1995, DOI: 10.1029/95JA00766.

Lu, G., D.N. Baker, R.L. McPherron, C.J. Farrugia, D. Lummerzheim, et al. Global energy deposition during the January 1997 magnetic cloud event. *J. Geophys. Res.*, **103 (A6)**, 11685–11694, 1998, DOI: 10.1029/98JA00897.

Luan, X., W. Wang, A. Burns, S. Solomon, Y. Zhang, and L.J. Paxton. Seasonal and hemispheric variations of the total auroral precipitation energy flux from TIMED/GUVI. *J. Geophys. Res.*, **115**, A11304, 2010, DOI: 10.1029/2009JA015063.

MacGorman, D.R., and W.D. Rust. *The electrical nature of storms*, Oxford University Press, New York, NY, USA, ISBN-10: 0195073371/ISBN-13: 978-0195073379, 1998.

Mackerras, D., M. Darveniza, R.E. Orville, E.R. Williams, and S.J. Goodman. Global lightning: total, cloud and ground flash estimates. *J. Geophys. Res.*, **103 (D16)**, 19791–19809, 1998, DOI: 10.1029/98JD01461.

Mathis, J.S., P.G. Mezger, and N. Panagia. Interstellar radiation field and dust temperatures in the diffuse interstellar matter and in giant molecular clouds. *A&A*, **128 (1)**, 212–229, 1983.

Matthews, G. Celestial body irradiance determination from an underfilled satellite radiometer: application to albedo and thermal emission measurements of the Moon using CERES. *Appl. Opt.*, **47**, 4981–4993, 2008, DOI: 10.1364/AO.47.004981.

Mathews, J.D., D. Janches, D.D.Meisel, and Q.-H. Zhou. The micrometeoroid mass flux into the upper atmosphere: arecibo results and a comparison with prior estimates. *Geophys. Res. Lett.*, **28 (10)**, 1929–1932, 2001, DOI: 10.1029/2000GL012621.

Maurette, M. *Micrometeorites and the mysteries of our origins*, Springer, Berlin, Heidelberg, Germany, ISBN: 978-3-540-25816-2, 2006.

McLandress, C. The seasonal variation of the propagating diurnal tide in the mesosphere and lower thermosphere. Part I: the role of gravity waves and planetary waves. *J. Atmos. Sci.*, **59 (5)**, 893–906, 2002.

McLandress, C., and W.E. Ward. Tidal/gravity wave interactions and their influence on the large-scale dynamics of the middle

atmosphere: model results. *J. Geophys. Res.*, **99 (D4)**, 8139–8155, 1994. DOI: 10.1029/94JD00486.
Meier, R.R. Ultraviolet spectroscopy and remote sensing of the upper atmosphere. *Space Sci. Rev.*, **58**, 1–185, 1991, DOI: 10.1007/BF01206000.
Meinel, A.B. The spectrum of the airglow and the aurora. *Rep. Prog. Phys.*, **14**, 121–146, 1951, DOI: 10.1088/0034-4885/14/1/305.
Mezger, P.G. The interstellar radiation field and its interaction with the interstellar matter. In: *Galactic and extragalactic background radiation*, **A92-24276**, Kluwer Academic Publishers, Dordrecht, The Netherlands, 63–73, 1990.
Mironova, I.A., K.L. Aplin, F. Arnold, G.A. Bazilevskaya, R.G. Harrison, A.A. Krivolutsky, K.A. Nicoll, E.V. Rozanov, E. Turunen, and I.G. Usoskin. Energetic particle influence on the earth's atmosphere. *Space Sci. Rev.*, **194**, 1–96, 2015, DOI: 10.1007/s11214-015-0185-4.
Miyashita, Y., Y. Miyoshi, Y. Matsumoto, A. Ieda, Y. Kamide, et al. Geotail observations of signatures in the near-Earth magnetotail for the extremely intense substorms of the 30 October 2003 storm. *J. Geophys. Res.*, **110**, A09S25, 2005, DOI: 10.1029/2005JA011070.
Mlynczak, M.G. Energetics of the mesosphere and lower thermosphere and the SABER experiment. *Adv. Space Res.*, **20 (6)**, 1177–1183, 1997, DOI: 10.1016/S0273-1177(97)00769-2.
Murcray, F.H. The spectral dependence of lunar emissivity. *J. Geophys. Res.*, **70**, 4959–4962, 1965, DOI: 10.1029/JZ070i019p04959.
Murcray, F.H., D.G. Murcray, and W.J. Williams. Infrared emissivity of lunar surface features 1. Balloon-borne observations. *J. Geophys. Res.*, **75 (14)**, 2662–2669, 1970, DOI: 10.1029/JB075i014p02662.
Newell, P.T., K. Liou, T. Sortirelis, and C.-I. Meng. Auroral precipitation power during substorms: a Polar UV Imager-based superposed epoch analysis. *J. Geophys. Res.*, **106 (A12)**, 28885–28896, 2001, DOI: 10.1029/2000JA000428.
Newell, P.T., T. Sotirelis, and S. Wing. Diffuse, monoenergetic, and broadband aurora: the global precipitation budget. *J. Geophys. Res.*, **114**, A09207, 2009, DOI: 10.1029/2009JA014326.
Ngwira, C.M., A. Pulkkinen, M.L. Mays, M.M. Kuznetsova, A.B. Galvin, K. Simunac, D.N. Baker, X. Li, Y. Zheng, and A. Glocer. Simulation of the 23 July 2012 extreme space weather event: What if this extremely rare CME was Earth directed? *Space Weather*, **11**, 671–679, 2013, DOI: 10.1002/2013SW000990.
Norton, O.R., and L.A. Chitwood. *Field guide to meteors and meteorites*, Springer, London, ISBN-10: 1848001568/ISBN-13: 978-1848001565, 2008.
Noterdaeme, P., P. Petitjean, R. Srianand, C. Ledoux, and S. López. The evolution of the cosmic microwave background temperature. *A&A*, **526 (L7)**, 1–5, 2011.
NRC. *Solar Influences on Global Change, National Research Council (U.S.), Committee on Global Change*, National Academy Press, Washington, DC, ISBN: 0-309-53812-2, 1994.
Oberheide, J., M.E. Hagan, R.G. Roble, and D. Offermann. Sources of nonmigrating tides in the tropical middle atmosphere. *J. Geophys. Res.*, **107 (D21)**, 4567, 2002, DOI: 10.1029/2002JD002220.
Orville, R.E., and D.W. Spencer. Global lightning flash frequency. *Mon. Wea. Rev.*, **107**, 934–943, 1979, DOI: 10.1175/1520-0493(1979)107<0934:GLFF>2.0.CO;2.
Oyama, S., K. Shiokawa, J. Kurihara, T.T. Tsuda, S. Nozawa, Y. Ogawa, Y. Otsuka, and B.J. Watkins. Lower-thermospheric wind fluctuations measured with an FPI during pulsating aurora at Tromso Norway. *Ann. Geophys.*, **28**, 1847–1857, 2010, DOI: 10.5194/angeo-28-1847-2010.
Palmroth, M., P. Janhunen, T.I. Pulkkinen, and H.E.J. Koskinen. Ionospheric energy input as a function of solar wind parameters: global MHD simulation results. *Ann. Geophys.*, **22**, 549–566, 2004.
Penzias, A.A., and R.W. Wilson. A measurement of excess antenna temperature at 4080 Mc/s. *Astrophys. J.*, **142**, 419–421, 1965, DOI: 10.1086/148307.
Pertsev, N., and V. Perminov. Response of the mesopause airglow to solar activity inferred from measurements at Zvenigorod Russia. *Ann. Geophys.*, **26**, 1049–1056, 2008, DOI: 10.5194/angeo-26-1049-2008.
Pollack, H.N., S.J. Hurter, and J.R. Johnson. Heat flow from the Earth's interior: analysis of the global dataset. *Rev. Geophys.*, **31 (3)**, 267–280, 1993, DOI: 10.1029/93RG01249.
Plane, J.M.C. Cosmic dust in the earth's atmosphere. *Chem. Soc. Rev.*, **41**, 6507–6518, 2012, DOI: 10.1039/c2cs35132c.
Platzman, G.W. An observational study of energy balance in the atmospheric lunar tide. *Pure Appl. Geophys.*, **137**, 1–33, 1991, DOI: 10.1007/BF00876887.
Price, C., J. Penner, and M. Prather. NO_x from lightning: 1. Global distribution based on lightning physics. *J. Geophys. Res.*, **102 (D5)**, 5929–5941, 1997, DOI: 10.1029/96JD03504.
Pulkkinen, T. Space weather: terrestrial perspective. *Living Rev. Sol. Phys.*, **4**, 5–60, 2007, DOI: 10.12942/lrsp-2007-1.
Pulkkinen, T.I., N.Y. Ganushkina, E.I. Kallio, G. Lu, D.N. Baker, N.E. Turner, T.A. Fritz, J.F. Fennell, and J. Roeder. Energy dissipation during a geomagnetic storm: May 1998. *Adv. Space. Res.*, **30**, 2231–2240, 2002, DOI: 10.1016/S0273-1177(02)80232-0.
Rakov, V.A., and M.A. Uman. *Lightning: physics and effects*, Cambridge University Press, New York, NY, USA, ISBN-10: 0521035414/ISBN-13: 978-0521035415, 2003.
Reach, W.T., P. Morris, F. Boulanger, and K. Okumura. The mid-infrared spectrum of the zodiacal and exozodiacal light. *Icarus*, **164 (2)**, 384–403, 2003, DOI: 10.1016/S0019-1035(03)00133-7.
Rostoker, G., and S. Skone. Magnetic flux mapping considerations in the auroral oval and the Earth's magnetotail. *J. Geophys. Res.*, **98 (A2)**, 1377–1384, 1993, DOI: 10.1029/92JA01838.
Sandford, D.J., H.G. Muller, and N.J. Mitchell. Observations of lunar tides in the mesosphere and lower thermosphere at Arctic and middle latitudes. *Atmos. Chem. Phys.*, **6**, 4117–4127, 2006, DOI: 10.5194/acp-6-4117-2006.
Schumann, U., and H. Huntrieser. The global lightning-induced nitrogen oxides source. *Atmos. Chem. Phys.*, **7**, 3823–3907, 2007, DOI: 10.5194/acp-7-3823-2007.
Sclater, J.G., C. Jaupart, and D. Galson. The heat flow through oceanic and continental crust and the heat loss of the Earth. *Rev. Geophys.*, **18 (1)**, 269–311, 1980, DOI: 10.1029/RG018i001p00269.
Sellers, W.D. *Physical climatology*, University of Chicago Press, Chicago, IL, USA, ISBN-10: 0226746992/ISBN-13: 978-0226746999, 1965.
Seppälä, A., P.T. Verronen, V.F. Sofieva, J. Tamminen, E. Kyrölä, C.J. Rodger, and M.A. Clilverd. Destruction of the tertiary ozone maximum during a solar proton event. *Geophys. Res. Lett.*, **33**, L07804, 2006, DOI: 10.1029/2005GL025571.
Silbergleit, V.M., M.M.Zossi de Artigas, and J.R. Manzano. Energy dissipation in substorms: plasmoids ejection. *J. Atmos. Solar Terr. Phys.*, **59**, 1355–1358, 1997, DOI: 10.1016/S1364-6826(96)00108-3.
Slavin, J.A., D.H. Fairfield, M.M. Kuznetsova, C.J. Owen, R.P. Lepping, et al. ISTP observations of plasmoid ejection: IMP 8 and Geotail. *J. Geophys. Res.*, **103 (A1)**, 119–133, 1998, DOI: 10.1029/97JA02136.
Slinker, S.P., J.A. Fedder, and J.G. Lyon. Plasmoid formation and evolution in a numerical simulation of a substorm. *Geophys. Res. Lett.*, **22 (7)**, 859–862, 1995, DOI: 10.1029/95GL00300.
Solanki, S.K., N.A. Krivova, and J.D. Haigh. Solar irradiance variability and climate. *Annu. Rev. Astron. Astrophys.*, **51**, 311–351, 2013, DOI: 10.1146/annurev-astro-082812-141007.
Sparrow, J.G., and E.P. Ney. Discrete light sources observed by satellite OSO-B. *Science*, **161 (3840)**, 459–460, 1968, DOI: 10.1126/science.161.3840.459.

Sparrow, J.G., and E.P. Ney. Lightning observations by satellite. *Nature*, **232**, 540–541, 1971, DOI: 10.1038/232540a0.

Stacey, F.D., and P.M. Davis. *Physics of the Earth*, 4th edn., Cambridge University Press, New York, NY, USA, ISBN-10: 1107394236/ISBN-13: 9781107394230, 2008.

Stanev, T. *High energy cosmic rays*, Praxis Publishing Ltd, Chichester, UK, ISBN-10: 3540406530/ISBN-13: 978-3540406532, 2004.

Stein, C.A., and S. Stein. A model for the global variation in oceanic depth and heat flow with lithospheric age. *Nature*, **359**, 123–129, 1992, DOI: 10.1038/359123a0.

Stephens, G.L., J. Li, M. Wild, C.A. Clayson, N. Loeb, S. Kato, T. L'Ecuyer, P.W. Stackhouse Jr., M. Lebsock, and T. Andrews. An update on Earth's energy balance in light of the latest global observations. *Nature Geosci.*, **5**, 691–696, 2012, DOI: 10.1038/ngeo1580.

Stern, D.P. Energetics of the magnetosphere. *Space Sci. Rev.*, **39**, 193–213, 1984, DOI: 10.1007/BF00173674.

Tanskanen, E.I., M. Palmroth, T.I. Pulkkinen, H.E.J. Koskinen, P. Janhunen, N. Ostgaard, J.A. Slavin, and K. Liou. Energetics of a substorm on 15 August, 2001: comparing empirical methods and a global MHD simulation. *Adv. Space Res.*, **36 (10)**, 1825–1829, 2005, DOI: 10.1016/j.asr.2004.05.013.

Tanskanen, E., T.I. Pulkkinen, H.E.J. Koskinen, and J.A. Slavin. Substorm energy budget during low and high solar activity: 1997 and 1999 compared. *J. Geophys. Res.*, **107 (A6)**, SMP 15-1–SMP 15-11, 2002, DOI: 10.1029/2001JA900153.

Taylor, S., J.H. Lever, and R.P. Harvey. Accretion rate of cosmic spherules measured at the South Pole. *Nature*, **392**, 899–903, 1998, DOI: 10.1038/31894.

Torr, M.R., D.G. Torr, M. Zukic, R.B. Johnson, J. Ajello, et al. A far ultraviolet imager for the international solar-terrestrial physics mission. *Space Sci. Rev.*, **71**, 329–383, 1995.

Trenberth, K.E., J.T. Fasullo, and J. Kiehl. Earth's global energy budget. *Bull. Amer. Meteorol. Soc.*, **90 (3)**, 311–324, 2009, DOI: 10.1175/2008BAMS2634.1.

Tsumura, K., J. Battle, J. Bock, A. Cooray, V. Hristov, et al. Observations of the near-infrared spectrum of the zodiacal light with Ciber. *Astrophys. J.*, **719**, 394–402, 2010, DOI: 10.1088/0004-637X/719/1/394.

Uman, M.A. *The lightning discharge*, **vol. 39**, Academic Press, Orlando, FL, USA, ISBN-10: 0080959814/ISBN-13: 9780080959818, 1987.

Usoskin, I.G., S.K. Solanki, and G.A. Kovaltsov. Grand minima and maxima of solar activity: new observational constraints. *A&A*, **471**, 301–309, 2007, DOI: 10.1051/0004-6361:20077704.

Vazquez, M., and J.M. Vaquero. Aurorae observed at the Canary Islands. *Sol. Phys.*, **267 (2)**, 431–444, 2010, DOI: 10.1007/s11207-010-9650-0.

Vial, F., and J.M. Forbes. Monthly simulations of the lunar semi-diurnal tide. *J. Atmos. Terr. Phys.*, **56 (12)**, 1591–1607, 1994, DOI: 10.1016/0021-9169(94)90089-2.

Wasson, J.T., and F.T. Kyte. Comment on the letter "On the influx of small comets into the Earth's atmosphere II: interpretation". *Geophys. Res. Lett.*, **14 (7)**, 779–780, 1987, DOI: 10.1029/GL014i007p00779.

Weiss, L.A., P.H. Reiff, J.J. Moses, R.A. Heelis, and B.D. Moore. Energy dissipation in substorms, *Proceedings of the First International Conference on Substorms, 23–27 March 1992*, 309–317, 1992, ESA SP-335.

Werner, M.W., and W.E. Salpeter. Grain temperatures in interstellar dust clouds. *Mon. Not. R. Astron. Soc.*, **145**, 249–269, 1969.

Wild, M., D. Folini, C. Schär, N. Loeb, E.G. Dutton, and G. K-Langlo. The global energy balance from a surface perspective. *Clim. Dyn.*, **40**, 3107–3134, 2013, DOI: 10.1007/s00382-012-1569-8.

Williams, D.L., and R.P. Von Herzen. Heat loss from the Earth: new estimate. *Geology*, **2 (7)**, 327–328, 1974, DOI: 10.1130/0091-7613(1974)2<327:HLFTEN>2.0.CO;2.

Willson, R.C., and H.S. Hudson. Solar luminosity variations in solar cycle 21. *Nature*, **332**, 810–812, 1988, DOI: 10.1038/332810a0.

Willson, R.C., and H.S. Hudson. The Sun's luminosity over a complete solar cycle. *Nature*, **351**, 42–44, 1991, DOI: 10.1038/351042a0.

Wright, E.L. Angular power spectra of the COBE DIRBE maps. *Astrophys. J.*, **496**, 1–8, 1998, DOI: 10.1086/305345.

Yang, H.G., and M. Ishiguro. Origin of interplanetary dust through optical properties of zodiacal light. *Astrophys. J.*, **813 (2)**, 1–9, 2015, DOI: 10.1088/0004-637X/813/2/87.

Zhang, X., J.M. Forbes, and M.E. Hagan. Longitudinal variation of tides in the MLT region: 1. Tides driven by tropospheric net radiative heating. *J. Geophys. Res.*, **115**, A06316, 2010a, DOI: 10.1029/2009JA014897.

Zhang, X., J.M. Forbes, and M.E. Hagan. Longitudinal variation of tides in the MLT region: 2. Relative effects of solar radiative and latent heating. *J. Geophys. Res.*, **115**, A06317, 2010b, DOI: 10.1029/2009JA014898.

Zipser, E.J. Deep cumulonimbus cloud systems in the tropics with and without lightning. *Mon. Wea. Rev.*, **122**, 1837–1851, 1994, DOI: 10.1175/1520-0493(1994)122<1837:DCCSIT>2.0.CO;2.

Zirker, J.B. Coronal holes and high-speed wind streams. *Rev. Geophys.*, **15 (3)**, 257–269, 1977, DOI: 10.1029/RG015i003p00257.

Cite this article as: Kren AC, Pilewskie P & Coddington O. Where does Earth's atmosphere get its energy? *J. Space Weather Space Clim.*, **7**, A10, 2017, DOI: 10.1051/swsc/2017007.